Post-analysis simulation of the collapse of an open sabo dam of steel pipes subjected to boulder laden debris flow

Toshiyuki Horiguchi, Vincent Richefeu

1. **Title**

Post-analysis simulation of the collapse of an open sabo dam of steel pipes subjected to boulder laden debris flow

2. **Author names and affiliations**

Toshiyuki Horiguchi[a], Vincent Richefeu[b*]
[a] *Department of Civil Engineering, National Defense Academy, Japan*
[b] *Université Grenoble Alpes, Laboratoire 3SR (sols, solides, structures, risques), UMR 5521, Domaine Universitaire BP53, France*

1. Introduction

Seventy percent of Japan is covered with hillslopes and mountainous regions including several torrential rivers, and, thus, Japan is a geologically fragile country. The land has been affected by large typhoons and torrential rain resulting in landslides and debris flows occurring annually (Ministry of Land, Infrastructure Transport and Tourism [MLIT], 2018b). Recently, a torrential rainfall event in the northern Kyushu area, Japan, occurred in July, 2017 and transported large volumes of driftwood as large woody debris (LWD) and approximately 40 people were reported as victims in Oita and Fukuoka (Marutani et al., 2017). Moreover, a torrential rainfall event occurred in central western Japan resulting from Typhoon Prapiroon that hit Hiroshima in July 2018; it resulted in instant collapse of a masonry check dam, and more than 200 people were injured (MLIT, 2018a).

Based on debris flow incidents, it is necessary to rapidly apply both tangible factors such as sabo dam facilities and intangible factors such as warning and evacuation programs. By analyzing several recent site investigation data regarding weather, a debris flow that exceeds the expected design load has been determined as the cas when the debris flow results in a larger external force than the present design load (National Institute for Land and Infrastructure Management [NILIM], 2016a, 2016b). This circumstance that suppresses the original performance was generated by the abnormal weather events, such as a large typhoon. Thus, it is indispensable to investigate the performance of existing facilities, and to evaluate the load carrying performance of sabo dams at full scale (Horiguchi & Katsuki, 2017; Ishikawa et al., 2018). The load carrying performance of a sabo dam is indispensable to examine whether it possibly withstand the impulsive load of a debris flow (Horiguchi & Katsuki, 2018).

Subsequently, an open sabo dam, as shown in Fig. 1a, was primarily constructed based on the Japanese sabo dam design guidelines (NILIM, 2016a, 2016b) in 2007. The open sabo dam facilities naturally allow routine bedload transport (Mizuyama, 2008). In addition, the trapping efficiency of the dam is enhanced by the boulder concentration mechanism in the front part of a debris flow (Armanini et al., 1991). Moreover, sabo dam facilities had never received large damage in Japan. However, Fig. 1b shows the broken sabo dam resulting from the debris flow generated in 2014 at Nagano

(Hiramatsu et al., 2014; Yamamoto & Toyota, 2016). The steel pipe of the crest is damaged owing to boulder impact. It was found that the structure couldn't withstand the impulsive load of an unexpectedly large debris flow load (Sonoda et al., 2016). Thus, it is indispensable to examine optimum evaluation method or the reproduction analysis of the debris flow to understand the load carrying performance of open sabo dams at real scale.

Many scientific papers have focused on load estimation (e.g., Hübl et al., 2009, 2017). They have to be examined to shed some light on the load-carrying performance of open sabo dams. The current design approach is based on a concept that considers fluid and rigid-body theories separately (Daido et al., 1994; Ikeya, 1978; Mizuyama, 1979): that is, it examines the flow of the fluid and that of the boulders independently, in a decoupled manner. The boulder collision load is based on the Hertz model (Hioki et al., 1973; Hirao et al., 1970). However, these approaches need to use safety factors, and they usually overestimate the impulsive load. Therefore, in extracting each point, the debris flow fluid force that is used is based on the mean quasi-static load, and the theory of the design was developed to evaluate debris flow load. However, the design approach does not necessarily comprise an acceptable load compared with real debris flow load sand experimental results. (Horiguchi et al., 2017). Moreover, parameters such as safety factors judged empirically affect the evaluation of debris flow loads.

The load evaluation methods in Austria, Switzerland, and France mostly use a theory based on fluid mechanics, and most cases utilize an empirical value of safety factor (Deymier et al., 1997; Federal Office for the Environment [FOEN], 2016; Hübl et al., 2017). Boulder laden debris flow has a lot of uncertainty in the estimation of the impact load owing to the boulders. Particularly, in the current design approach, boulder impact load is one tenth of the force evaluation obtained from the Hertz model, and the perspective of dynamics is misaligned (Mizuyama, 1979; Osanai et al., 2010). Moreover, the design approach was used originally for closed sabo dams, and the characteristics of open sabo dams using hollow pipes are exceedingly different. Further, open sabo dams have complex shapes, and the change of impact loads affects the change of the contact plate (Horiguchi & Komatsu, 2018). It is considered difficult to correctly use the current design approach. An impulsive load experiment was done to obtain a load evaluation for open sabo dams; an impulsive load occurs once, and the

load represents a static load only for water and sediment (Miyoshi & Suzuki, 1990; Mizuyama et al., 1985). Thus, it is considerably difficult to ascertain this part of the design approach to be applied in the load evaluation. Therefore, the evaluation of debris flows should not only be done at an experimental scale, but also the study requires that the impulsive load evaluation be done for a real scale debris flow.

Previous studies present some methods for debris flow load evaluation at a real scale. The real-scale cases involve different geographical features, and the evaluation is significantly varied. The studies examine the expected debris flow to evaluate the impulsive load, but this impulsive load evaluation is not currently used as an approximation process because of the large difference in the actual dynamic loading (Osaka et al., 2013).

One of the presumed load equations has been examined with respect to the equation modeled at real scale to determine the safety parameters based on the load obtained from the experimental data. However, this equation has not come to be used in practical cases because presumed load and real debris flow load differs by more than 20% (Hübl et al., 2017). Therefore, several analytical examinations are used to estimate the debris flow load against an open sabo dam (Horiguchi et al., 2018; Rimbock, 2004).

Also, evaluation of the load using the discrete element method (DEM) results from the computed contact forces of the spherical elements on a rigid body plane. This impact load evaluation is performed under dry conditions, and it solely evaluates the boulder contact load (Albaba et al., 2015; Canelas et al., 2015). Moreover, the method of flow and the shape of boulder are examined. Thus, a DEM is employed to evaluate load, and the reliability of the applicability of this approach is validated. DEMs have lately used more complex shapes, and more relevant methods are increasingly being developed. These methods examine the movement of complicated shapes such as polygonal elements (Falcetta, 1985; Johnson, 1989; Richefeu & Villard, 2016). This clump element consists of a plane element, a spherical element, and a cylindrical element, and the complexity of the shapes is expandable. The current study examines the problem of energy dissipation, and the reproducibility of an original movement characteristics is evaluated for the spring model with respect to the hardness of the material's physical properties. However, there are studies that focus on the micro perspective scope using high technology methods. Real scale debris flows has not yet

been examined from a macro perspective.

To evaluate a damaged structure such as in the case of Nashizawa debris flow disaster, it is important to reproduce the mixture of water and boulders. Recently, several studies have been done using fluid analysis methods. The fluid analysis is a Euler-Lagrange coupling and the interpretation of the artificial viscosity term is exceedingly difficult to understand relative to practical methods (Beppu et al., 2011; Suzuki & Hotta, 2016). Moreover, the collaborative analysis of the sabo dam and debris flow has been examined in a few studies. Quite a few papers exist that infer the damage process regarding how the structure receives external force (Horiguchi & Katsuki, 2015).

The current study suggests a damage verification process method of steel pipe open sabo dams influenced by large-scale boulder laden debris flows using a DEM. The parameter decision process utilizes site investigation of the Nagiso debris flow. First, the site investigation process is explained to obtain parameters such as the debris flow peak discharge, debris flow velocity, and fluid force. Second, a real scale numerical analysis is done to explain the damage mechanism of an open sabo dam. Finally, the analysis results are utilized to consider the structural fragility through a comparative result of "Reproduction analysis" and "Reinforced analysis".

2. Bouldery debris flow that occurred in Nagano, Nagiso-cho on July 8, 2014

2.1. Overview of the disaster

The debris flow caused high damage including 1 dead and 3 injured people, 25 damaged houses, and damage to route No. 19 and the Japan Rail (JR) Chuou Main Line (Hiramatsu et al., 2014). Three existing sabo dams set in the Nashizawa watershed experienced high damage owing to boulder laden debris flows. Moreover, damage due to inundation above floor level or under floor level flood, traffic obstruction, etc. occurred in the Kiso region. Nagiso is located on the south side of the Kiso valley, and on the east side of Kiso mountain range including Mt. Kisokoma and Mt. Ena on the northwest side of Mt. Mitake. The Kiso River flows between the high mountains to the west. The Nashizawa debris flow occurred at the confluence of the Kiso River where it is the source river of Southern Mt. Kiso (Fig. 2). The drainage area of the Nashizawa

District is 3.35 km^2, and the average bed slope is approximately 1/3.5. Kiso town is widely spread out with a gradient of 30° or more, and there are several rapid stream reaches with a river bed slope of 10° to 30° toward the upstream of Nashizawa.

2.2. Application of standard debris flow magnitude methods

The plain landslide scar was not confirmed with respect to the uppermost part of the debris flow between the origin of the debris flow and the Nashizawa River basin (Fig. 2). Moreover, the uppermost part of debris flow of the Syo-Nashizawa Swamp basin was confirmed with respect to the erosion of the river bed. The land surface runoff was generated by the downpour in the swamp. The sediment that had accumulated in the swamp was eroded by the tractive force of the surface runoff. Therefore, it is observed that the debris flow occurred under this circumstance. Because the generation origin of the river bed was a steep gradient of 30-35°, the debris flow velocity is exceedingly rapid. The exposed boulders are spread due to the erosion of the river bed. The sediment was accumulated upstream of the small check dams. Further, the small check dams collapsed. The released sediment is accumulated after causing erosion, and the accumulated sediment including the boulders remain in the river channel, which primarily exhibits a linear gradient.

The debris flow directly hit the first Nashizawa sabo dam, and the upper parts of the crest flowed out because of the failure of the coupling join. The remaining steel pipe components captured the boulders and sediment. Subsequently, the erosion control domain of the first Nashizawa sabo dam was mostly empty before the debris flow occurrence. The ground elevations measured via aerial laser measurement after the debris flow was generated and compared to the ground measured in 2008. The capturing volume was assumed to be approximately 5,000 m^3 (Fig. 3) (the designed/planned quantity of sediment capture is 24,500 m^3). Moreover, the eroded river bed and river banks is between the first Nashizawa sabo dam and the confluence point because of the narrow valley width and straight channel.

2.3. Failure event re-analysis

The external force is estimated in this section. The debris flow peak discharge was determined based on a comparison of three methods, and the greatest value was used.

These methods follow the concept of methods based on the amount of the precipitation, and the method based on the volume of outflow sediment in design. Each method is illustrated in the following subsections (Mizuyama & Semoo, 1984; Mizuyama & Uchara, 1984; Ou et al., 1991).

2.3.1. Debris flow peak discharge based on amount of precipitation in design

$$Q_{sp} = \frac{C^*}{C^* - C_d} Q_p \quad (1)$$

where Q_{sp} is the debris flow peak discharge (m^3/s), Q_p is related discharge of only water C^* is the volume fraction of sediment deposited on the river bed ($C^* = 0.6$ in design), C_d is the volume fraction of debris ($C_d = 0.34$ under the present design). The debris fraction is obtained as follows (Takahashi, 2004):

$$C_d = \frac{\rho_w tan\theta}{(\sigma - \rho_w)(tan\varphi - tan\theta)} \quad (2)$$

where σ is the density of gravel ($\sim$2,600 kg/m^3), ρ_w is the density of water ($\sim$1,200 kg/m^3), φ is the internal friction angle (°) of sediment deposited on a river bed (from 30° to 40°), and θ is the river bed gradient (°).

2.3.2. Debris flow peak discharge based on site investigation (before disaster)

The debris flow peak discharge is defined as follows:

$$Q_{sp} = \frac{1}{100} \sum Q \quad (3\text{-a})$$

where the total discharge of debris flow $\sum Q$ (m^3) is itself defined by:

$$\sum Q = \frac{V_{dpq} C}{C_d} \quad (3\text{-b})$$

where V_{dpq} is the volume of sediment (m^3) predicted to be in the runoff from a single wave debris flow (including voids) and C is the volume of unstable sediment in the main bed river ($C = 9{,}513$ m^3 from site investigation before the event occurrence). Therefore, the debris flow peak discharge was found to be $Q_{sp} = 167.9$ m^3/s.

2.3.3. Debris flow peak discharge based on investigation data (after disaster)

The debris flow velocity and depth calculation method is illustrated as follows. The

method uses the continuous equation and Manning's equation. The debris flow peak discharge is given by:

$$Q_{sp} = BhU \tag{4}$$

where B *is* debris flow width (here 12.0 m), h *is the* debris flow depth (m), and U is a flow velocity (m/s) of the debris flow defined by:

$$U = \frac{1}{n}\left(h^{2/3} sin^{1/2}\theta\right) \tag{5}$$

with

$$h = \left(\frac{nQ_{sp}}{Bsin^{1/2}\theta}\right)^{3/5} \tag{6}$$

where n is Manning's roughness coefficient (design standard = 0.1 $\sec \cdot m^{1/3}$) and θ is the river bed gradient (°).

The roughness coefficient is larger than in the case of clear water, and in a natural river course it is 0.10. The velocity and depth of the debris flow are obtained for the front part of the flow. Therefore, the debris flow depth and velocity were found to be $h = 1.99$ m and $U = 7.01$ m/s. Subsequently, the debris unit weight ρ_d (kN/m^3) is obtained by the following equation (Takahashi, 2004):

$$\rho_d = \sigma C_d + \rho_w(1 - C_d) \tag{7}$$

The debris flow fluid force F per unit of width (kN/m) is estimated using the following equation:

$$F = K_h \frac{\rho_d}{g} hU^2 \tag{8}$$

where g is the acceleration of gravity, and K_h is a safety factor (here $K_h = 1.0$).

2.3.4. Final determination of debris flow peak discharge

On the other hand, the data obtained from site investigations are predicted to be the origin of the debris flow. The peak discharge is examined in the upstream reaches. The data was calculated for each parameter using the Manning's equation based on the debris flow survey. The estimation of debris flow utilized four small check dams set in the upstream reaches of the first Nashizawa sabo dam, and each point is compared to estimate the debris flow. This approximately assumes uniform flow, the average

velocity using Manning's equation, and the cross sectional area to calculate the discharge as follows.

$$Q = AU \tag{9}$$

$$U = \frac{1}{n} R^{2/3} \sqrt{I} \tag{10}$$

where Q is the discharge, A is the cross sectional area, I is the river bed gradient, and R is the wetted perimeter.

The longitudinal inclination of each cross section uses the database of the Ministry of Land, Infrastructure Transport and Tourism (MLIT), and 100 m is the average longitudinal inclination of the stream from the first small check dam to the fourth small check dam. The cross sectional area of the river is the cross sectional area of each measurement position. The first small check dam is the closest to the first Nashizawa sabo dam and it is used to select the initial data, but this check dam completely collapsed. Therefore, the data selected for the origin of the debris flow was from the secondary small check dam. The result of the site investigation is calculated as discharge ($Q = 733$ m^3/s) and flow velocity ($U = 8.3$ m/s) from the cross sectional area ($A = 89$ m^2), wetted perimeter ($R = 2.27$ m), and hydraulic radius (39 m).

Therefore, the debris flow peak discharge is assumed to be 733 m^3/s at the first Nashizawa sabo dam. The possible velocity and height of the debris flow was predicted at the point of the Nashizawa sabo dam. Table 1 lists the data used to estimate the debris flow. Therefore, the debris flow depth is 3.3 m, and the debris flow velocity is 9.7 m/s. The estimated debris flow characteristics were determined to utilize the results of the site investigation data. Because the results obtained from the site investigation are the largest debris flow peak discharge among the ones considered. This concept always is utilized in Japan. Table 1 lists the calculation of the results for the design. The debris flow load is evaluated to use the information obtained from a site investigation.

The representative boulder was selected on basis of the boulders obtained from zone indicated in Fig. 4. In addition, the boulder investigation was done to determine the opening size of the open sabo dam. As points 200 m between up- and down-stream are considered for the sabo dam setting point, 100 or 200 boulders are selected at random in this region. The grain curve is plotted to use the average of three side lengths (long side, short side, and middle side) of the gravel. The parameter of this curve is defined as the

maximum boulder size (d_{95}). However, the gravel sampled at the investigation sites is listed in Table 2. These site investigations were checked for the boulders flowing from the dam after debris flow because of the collapse of the sabo dam. Thus, it is assumed that the maximum diameter of the boulders distributed from the first Nashizawa sabo dam in the upstream is used (Fig. 2).

2.4. Damage mechanism of the first Nashizawa sabo dam after site investigation

The damage mechanism of the sabo dam is estimated based on the results of the site investigation (Fig. 5). It is believed that the fluid force acted on the section of spillway because of local deformation of each part and the upper structural member of the crest in each section. Because there are signs of boulder collision on the vertical structural members from the crest to the bottom and boulder trace remained at the top of the concrete crest part. Accordingly, the upper structural member experienced large local deformation (Fig. 5a). The coupling joint was broken, and simultaneously the upper structural member gradually collapsed owing to the boulder collision in the upper of the crest while the boulders were overtopping the dam (Fig. 5b). It is assumed that the sediment is caught up to the crest parts of the spillway. However, once the trapped debris flow caused the coupling joint parts of the uppermost structural members to collapse, the trapped debris flow burdened the other joints. It is believed that the top part of the dam suffered intense damage (Figs. 5c and 5d). However, according to consideration based on the presumed damage mechanism, the structural members received a larger external force than expected in the design. The whole shape of the structure could not be maintained, but the trapping function was maintained to continue to entrap sediment.

Therefore, the trapping function was demonstrated to have a redundancy effect (Fig. 5e). However, the boulders that pass through the spillway broke the crest members after trapping all the sediment. The boulders acted on the crest structural member over and over (Fig. 5f)**.** Therefore, it is assumed that the structural member deformation was the reason for the damage.

3. Numerical model

3.1. Applied discrete element method

The DEM applied is quite classic in its numerical scheme. In particular, the rigid elements (boulders) are spheres and their motions and interactions obey Newton's laws. The current model (Horiguchi & Katsuki, 2017; Horiguchi et al., 2018) provides some specific features that are listed and summarized as follows.

1) In the boulder-boulder motion, normal and tangential contact forces are obtained from linear springs in series with dashpots that allow for the dissipation of energy. The dissipation of energy also is achieved by Coulomb friction. The choice of the related parameters will be specified subsequently.

2) The boulder-pipe tube contact forces are obtained in a similar manner, but the choice of parameters was modeled by comparison with finite element method (FEM) simulations.

3) In addition to gravity, the boulders experience a drag force field that emulates a steady flow. This flow takes place in a channel with a slope and width similar to experimental conditions. The initial velocity,U_0, and initial water depth, h_0, are set in accordance with site investigation data. The drag coefficient was set to 0.49 and the Reynolds number was in the range of 10^3 to10^5; Table 3.

4) Only the largest boulders are included in the model because the influence of the smallest is negligible. The sediment grading curve was obtained from the site investigation.

5) The roughness of the river bed is accounted for by setting fixed a rigid element that produces a hilly slope (Adachi, 1964).

6) The open sabo dam is modeled with pipe tubes connected with joints as described in the following Section.

3.2. Junction node model

The hollow pipes are modeled as elastic beams where deformations are concentrated in the nodes that connect those (Horiguchi et al., 2018). Each node can be pictured as 3 regular springs and 3 angular springs. These forces and moments are driven by the following incremental relation:

$$\tilde{\boldsymbol{S}}^{i+1} = \tilde{\boldsymbol{S}} + \boldsymbol{k}^i \cdot \Delta \boldsymbol{q}^i \tag{11}$$

where $\tilde{\boldsymbol{S}} = (F_x, F_y, F_z, M_x, M_y, M_z)^T$ is the internal force vector composed of the components of internal force and moment, $\Delta \boldsymbol{q} = (q_x, q_y, q_z, \theta_x, \theta_y, \theta_z)^T$ is the increment of displacement and rotation, $\dot{\boldsymbol{\iota}}$ is the step number used in the explicit integration scheme, and $\boldsymbol{k}$ is the stiffness matrix. This stiffness matrix expresses as each rigidity value is obtained from the following equations:

$$\boldsymbol{k} = \begin{pmatrix} k_x & 0 & 0 & & & \\ 0 & k_y & 0 & & \mathbf{0} & \\ 0 & 0 & k_z & & & \\ & & & k_{\theta x} & 0 & 0 \\ & \mathbf{0} & & 0 & k_{\theta y} & 0 \\ & & & 0 & 0 & k_{\theta z} \end{pmatrix} \tag{12}$$

with

$$k_x = \frac{2E_pA_t}{L_i+L_j}; \quad k_y = k_z = \frac{2}{L_i+L_j}\frac{E_pA_t}{2(1+\nu)}; \quad k_{\theta x} = k_{\theta y} = k_{\theta z} = \frac{2E_pI_t}{L_i+L_j} \tag{13}$$

where E_p is Young's modulus of the constitutive material, ν is the Poisson coefficient, $L_i$and L_j are the lengths of connected tubes i and j, A_t is a cross sectional area, and I_t is the second moment of this cross section.

No distinction is made between each rotation axis (same second moment) and this assumption did not significantly affect the computational results. It is worth noting that the pipe tubes are able to stand both tensile and compressive forces. Also, each node can be disconnected, which corresponds to an irreversible rupture. Some other parameters are, thus, also involved to monitor the failure: the elongation (expressed in percent) and the strength at breakage. In addition, the current study uses a constitutive law to express the fragility between the elements. Thus, the normal direction and shear direction are separated beyond the boundary condition.

4. Replication of the actual disaster by simulation

4.1. Calibration of the model parameters

4.1.1. Parameters of the joints: sectional partition method

The steel pipes in an open sabo dam are considered in safety assessment regarding the

flange in the present design, and the performance of flanges and coupling joint parts doesn't generate an unbalance in the load carrying capacity as for structural characteristics. So they carry nearly 75% of the capacity compared to the other elements of the structure in the present design. But, the parameters outlined in Section 3.2 are not straightforward to establish, in particular because of the arbitrariness of the boundary conditions. Also, the compression part exerts stresses on the flange-bolt assembly while the tension part only acts on the bolts; these two parts are separated by the neutral axis whose position is affected by the curvature of the members (Fig. 6). Therefore, the DEM parameters were solved by using a sectional partition method. Flange and bolts (S10T, M22 in the Japanese industrial standard) of coupling joint were calculated to estimate the stress distribution using the sectional partition method. The bolt part is simplified, and it is connected with the spring model (Fig. 7). The neutral axis position was estimated accordingly.

This process was repeated iteratively, as depicted in the flow chart of Fig. 8, because the surface to be considered is not the same in the compressive and tensile parts (the latter being helped only by the bolts). The iterative procedure resulted in the concerned curvature (bending angle) and it allowed a decision to be made on the stiffness, and the fracture parameters were adjusted on the basis of energy considerations (Fig. 9). The parameters that reflect the characteristics of the structure are listed in Table 4. In addition, the upstream secondary tubular elements are susceptible to local deformation (dents) in the form of compression buckling insertion. In order to get as close as possible to the real situation in a disaster, the characteristics of the concerned parts, therefore, differ from the other parts at the joint nodes. For a tube, the so-called dent displacement, δ_d, can be related to the load, P, thanks to the modified Ellinas equation (Ellinas & Walker, 1983; Hoshikawa et al., 1995) that reads:

$$P = \frac{K\sigma_{y,d}t^2}{4}\left(\frac{\delta_d}{D}\right)^{\beta} \tag{14}$$

where P is the load, K is an experimental coefficient ($K = 161(D_0/D)^{0.11}$, D_0 being the diameter of boulder which is set to 100 mm in the design phase), t is the thickness of the hollow steel pipe (mm), $\sigma_{y,d}$ is the dynamic stress yield of the hollow steel pipe (N/mm^2), (it is up to 20% greater than the static yield stress), D is the external diameter of the hollow steel pipe (mm), δ_d is the dent deformation (mm), and β is an

experimental dimensionless coefficient ($\beta = 0.8$).

The stiffness used for linear springs in the DEM can, however, be approximated as shown in Fig. 10 where a small plastic zone can also be noticed. It was added following on-site observations by noticing that δ_d/D = 95% (it corresponds to δ_d = 584 mm). The boulder that contacted the front of a steel tube had a diameter of approximately 3.8 m (estimated from the collision trace). This is in good agreement with the estimation of debris flow fluid force as shown in Fig. 11.

4.1.2. Parameters for boulder interactions

The normal direction of the spring between the elements was predicted from the analyzed data, where the value is obtained from the case of contact of boulder model and the steel pipe in the FEM analysis result. Moreover, the shear direction stiffness is calculated as outlined as follows. The spring constant of the DEM introduces a certain value utilizing the following equation, which uses the pulse wave propagation of an elastic wave from the linear approximation method for a wave theory.

$$K_n = \frac{\pi\rho}{4}V_p^2 \text{ and } K_s = \frac{\pi\rho}{4}V_s^2 \tag{15}$$

with the primary/longitudinal and secondary/transverse waves respectively given by:

$$V_p = \sqrt{\frac{\lambda+2G}{\rho}} \text{ and } V_s = \sqrt{\frac{G}{\rho}} \tag{16}$$

where $G = E/(2(1+\nu))$ is the shear modulus, $\lambda = E\nu/((1+\nu)(1-2\nu))$ is the constant of Lame expressed as a function the Young's modulus *E*, Poisson's ratio ν, and ρ is the density of elements.

The ratio of the shear direction spring constant (K_s) and normal direction spring constant (K_n) can be related to Young's modulus and to Poisson's ratio:

$$\frac{K_s}{K_n} = \frac{G}{\lambda+2G} = \frac{1-2\nu}{2(1-\nu)} \tag{17}$$

Generally, the Poisson's ratio for a boulder is $\nu = 0.23$, and so, $K_s/K_n = 0.35$ (Hakuno, 1997).

The damping of the collisions between the boulders is achieved by means of normal and tangential viscosity (dashpot coefficients c_n and c_s, respectively) in addition to the springs. These dashpots are essential for the proper stabilization of the dynamic method and they were mainly considered to damp elastic waves that propagate

through the flowing mass. Since the dashpot coefficients involve a critical value above which physics becomes inappropriate, a damping ratio h defined in the range [0; 1[(h = 0.8 was used) is introduced:

$$c_n = 2h\sqrt{m_{eff}K_n} \text{ and } c_s = 2h\sqrt{m_{eff}K_s} \quad (18)$$

where $m_{eff} = m_i m_j/(m_i + m_j)$ is the effective mass of the colliding boulders i and j.

In addition to the viscous dissipation, the Coulomb friction also acts between the boulders. The friction coefficient was set to 0.404, which correspond to a friction angle of 22° (Duran, 1999).

Table 3 lists the analysis parameters. The channel slope and element conditions are equivalent to the experimental conditions.

4.2. Analysis model

Figure 12 shows a schematic of the analysis model and each initial location. Each initial position is located in the study area and the debris flow directly flows down from the investigation site (Figs. 2 and 3), and the position located 200 m away from the sabo dam model is the initial position of the debris flow. The boulder model is based on the boulder investigation (Fig. 4), and the fitting curve utilizes uniform random numbers. Subsequently, the volume is based on the trapped volume from the site investigation data. Table 4 indicates each spherical volume. The open sabo dam model is illustrated in Figs. 13a and 13b. The sabo dam model has a height of 12.0 m, and a width of 10.0 m based on the real shape design (Fig. 13c). Each member model constitutes a clump model and connect spring as shown in Fig. 13d. In addition, the roughness model is used to express the real ground, and the model interval is determined using the Adachi (1964) equation. The analysis is done using "Reproduction analysis" and "Reinforced analysis". The objective of this compared model is that the analysis examines a reinforced joint analysis because of several causes of breaking coupling joints regarding a steel pipe, open sabo dam. "Reproduction analysis" means the DEM considers the weak components of coupling joints. "Reinforced analysis" means the DEM considers the reinforced coupling joint. The reproduction analysis reproduces the damaged sabo dam due to debris flow, and this model reproduces an actual disaster situation. The reinforced analysis replaced the stiffness of the hollow pipe, and the coupling joint part

was reinforced. Therefore, the model considers the same condition except the coupling joint.

4.3. Damage reproduction simulation

Figs. 14 and 15 show each case of the analysis results. Fig. 14 demonstrates the reproduction analysis that reproduces the joints. Fig. 14a determines the initial time ($t = t_0$) as the time when the debris flow is located 6 m away from the front of the open sabo dam. Fig. 14b shows the time when the debris flow comes in contact with the open sabo dam ($t = t_0 + 2$ s). Fig. 14c shows the front part of the debris flow when it collides with the rear crest of the dam. The upper member of the secondary part deforms largely at $t = t_0 + 7$ s. Therefore, it largely deforms the steel in the upper part immediately before damming up the boulders, and the steel part experiences high stress concentration. In addition, Fig. 14d shows the damage near the crest, i.e. the damage of the steel part. Moreover, the coupling joint of the first part experiences some damage when damming up the debris flow and a large load is generated in the lower direction, and the damage results in shear failure. Additionally, this situation collapses the steel in the upper part. This circumstance separates the coupling joint and the secondary part concentrates the load and is forced to separate the upper part. Fig. 14e represents entire process of damage and the decreased load carrying of the secondary structural members ($t = t_0 + 14.5$ s). This structure does not maintain its initial shape. The structure cannot maintain the redundancy of the entire structural shape, and the steel of the upper part moves downstream. Fig. 14f shows that the debris flow in the top part flows behind the dam. However, in the bottom part, the debris flow is trapped demonstrating the effect of catching. Figure 15 shows the result of the reinforced analysis. In Figs. 15a and 15b the structure withstands the impact load from the debris flow. Figure 15c shows the center part of the entire structure owing to debris flow. The analysis result indicates smaller deformation than for the reproduction analysis, and the debris flow does not dam up. In Fig. 15d, the upper part of the steel is largely deformed, but the structure does not collapse. The dam does not break, though the debris flow stops after this (Figs. 15e and 15f). Considering only the strength of the steel material, it is indicated that the dam never experiences significant damage. Therefore, a device that significantly

increases the strength for the coupling part is necessary.

4.4. Evaluation of load-carrying performance

Fig. 16 shows the relations between load and time of contact force. This result is obtained with regard to hollow steel. Figure 16a shows the lower part of the coupling joint in comparison with the reinforced analysis. The blue line represents reproduction analysis, and the red line represents reinforced analysis. The result ($t = t_0 + 3$ s) demonstrates a larger load than the reinforced analysis. Also, P_{1max} is larger than P_{2max} (where 1 and 2 are the reproduction and reinforced analyses, respectively, and max mean maximum), though the analyses consider the same condition of debris flow. Because the upper part and lower part support impulsive load from the debris flow, and the total load for the upper and lower part in Fig. 16 is the same value. The maximum load ($t = t_0 + 11.3$ s) is 6,245 kN, when the crest part of the sabo dam was significantly damaged in the debris flow. Immediately the load decreased because of the breakable structural shape, and the reproduction analysis did not sustain the debris flow load. Moreover, the estimated debris flow fluid force is 520 kN/m in site investigation result and the reproduction analysis yielded 520.4 kN/m in the numerical analysis, and the analysis result is in agreement with the estimated value.

On the other hand, the open sago dam in the reinforced analysis withstands the debris flow load as it increases by the end of the calculation time. The maximum load ($t = t_0 + 20.9$ s) is 5,709 kN. Because the reinforced analysis is done under unbreakable circumstances, another member compensates for the debris flow load. Therefore, if only structural changes in the joints of the hollow pipes are made, the structure significantly improves its load carrying performance. The impulsive load differs for each structural member, and structural component stiffness is largely influenced. The maximum load in the reproduction analysis is larger than the one in the reinforced analysis. Because a few structural components have already broken, and other structural components must support the impulsive load.

Further, Fig. 16b shows the relations between the load and time in the upper part. The reproduction analysis demonstrates the maximum load ($t = t_0 + 9.5$ s) when the debris flow dams up in the upper part of the crest. The maximum load is 9,292 kN. The

reinforced analysis increases the load in damming up the debris flow ($t = t_0 + 24.3$ s). The maximum load is 14,624 kN. The reinforced analysis deformed a little, but the structure withstands the debris flow load because the model utilized the hollow steel against the coupling joints. Therefore, there is a possibility for the coupling joint to be indicated as the primary factor, i.e. a weak part. In addition, it is believed that if the coupling joint is stronger than the carrying load, a resilient structure would be expressible. Thus, it is exceedingly indispensable to improve the coupling part.

Moreover, Fig. 17 shows the broken structural member in detail. The coupling joint was first broken in the structure. This result differs from the estimation of the site investigation data, but, it is believed that the primary factor indicated the possibility of a broken coupling part. Regarding the large deformation of the secondary member, the circumstance just considers the maximum load in the reproduction analysis. Generally, the analysis result demonstrates the characteristics of the steel pipe structure, and the steel pipe open sabo dam exhibits a redundancy effect because of the complicated shape owing to the use of hollow pipes, and the entire dam was not broken. The broken structure effectively traps the debris flow (∼5,000 m^3).

Finally, the numerical study used real investigation data, and it is thought that the discharge, boulder size, volume, and so on largely influence the impulsive load. The numerical evaluation obtained sufficient analysis results to guaranty the reliability of the data in the survey results. On the other hand, it is thought that an open sabo dam with enlarged trapping volume is necessary for trapping boulders at the downstream to suppress overflow of debris flows.

5. Discussions

The current study evaluates the load carrying performance of the open sabo dam that experienced debris flow using a site investigation. However, the design method remains unclear for designer or practitioner. It is difficult to estimate an impulsive load due to bouldery debris flow, and the mechanism is complicated. The evaluation method must be evaluated to improve the design standard for steel pipe open sabo dams.

5.1. Boulder collision load evaluation and debris flow fluid force

Present Japanese design uses quasi-statistic load evaluation. In addition, the design method considers boulder collision load evaluation and a debris flow fluid force equation. Although debris flow simultaneously generate boulder movement and following sediment, the mechanisms of the fluids and rigid bodies are not fully coupled. Also, the larger value is adapted in the present design. However, it is difficult to decide the maximum boulder size (d_{95}) in the site investigation, and a 1 m boulder was used based on empirical data. Therefore, debris flow fluid force was almost calibrated by considering a safety factor. The novel design standard of the water-boulder coupling formula is suggested to predict the accurate evaluation of impulsive load. The proposed method is the coupling method between fluid force and boulder collision, and it will be improved by collecting local disaster data and reproducing events to yield a lot of knowledge on the proposed method in the future.

5.2. The design method of steel pipe open sabo dams

In the present sabo dam design, the steel pipe was analyzed by using the modified Ellinas equation (Hoshikawa et al., 1995), Eq. 14, given as follows.

$$E_M = P\delta_d \tag{19}$$

where E_M is the global energy absorption by beam deformation, and δ_d is the local deformation, the last variable being expressed as follows.

$$\delta_d = D\left\langle \frac{16}{LKt^2}\left\{D^2 t + \frac{4}{3}\left[ab^2 - (a-t)(b-t)^2\right]\right\}\right\rangle^{1.25} \tag{20}$$

where a is the long radius of an ellipse ($a = D/[2(1-\alpha^2/4 - 3\alpha^4/64 - 15\alpha^6/768)]$, $\alpha^2 = 1-(b/a)^2$), b is the short radius of an ellipse ($b = (D-\delta_d)/2$), and the last variable being expressed as follows.

$$P = \frac{4}{L}(M_{PA} + M_{PC}) \tag{21}$$

where L is the span length, M_{PA} is the plastic moment at the fixed end ($M_{PA} = D^2\sigma_{y,d}t$), M_{PC} is the plastic moment at the center of the fixed beam ($M_{PC} = (4/3)\sigma_{y,d}\left\{ab^2 - (a-t)(b-t)^2\right\}$), δ_{Pa} is the limit of plastic deformation ($\delta_{Pa} = 2\theta_{Pa}/L$), and θ_{Pa} is the limit of plastic rotation ($\theta_{Pa} = 1.355t/D$).

The equation utilized estimated values based on local deformation between pipes and the load cell. This design is based on empirical data, and not related to span length,

and the flange and the coupling joint is similarly computed. There are still many questionable points in many areas about how to assess them. Therefore, it is hoped that the method which is suitable for each site and the span length and the joint can be evaluated. In addition, it is necessary to examine the performance evaluation of the entire structure because the evaluation of the impact load on the entire structure is unclear. The shape of the structure is influenced the load carrying performance, but the optimum structure shape is not examined in the current study. In the future, two concepts of evaluation for the local evaluation and the overall structure are desirable.

6. Conclusions

The current study proposed a damage verification method to determine the primary damage factors for an open sabo dam. The DEM parameters were determined based on debris flow data obtained from the site investigation of a debris flow disaster, and the proposed method reproduced the open sabo dam experiencing damage of the coupling joint in the Nagiso debris flow disaster. Subsequently, the impulsive load was predicted, and the cause of damage was considered.

1) The estimated debris flow fluid force is larger than the debris flow fluid force expected in design, and it was considered that the debris flow was the unexpected load.
2) The study estimated the debris flow peak discharge, velocity, debris flow fluid force, etc. using the Japanese sabo dam design standards after the debris flow disaster.
3) The proposed method qualitatively reproduced the circumstances of the open sabo dam experiencing damage owing to boulder laden debris flow in a real disaster.
4) The DEM parameters were determined based on the site investigation and the analytical results generally were in agreement with the estimated debris flow load obtained from the site investigation.
5) As for the damage circumstance of the structure, the coupling joints of the local weak point first collapsed and all of the structural shapes gradually deformed in the analysis. It is observed from this analytical result that the first Nashizawa sabo dam initially collapsed at the coupling joint.
6) However, the open sabo dam exhibits a redundancy effect owing to its complicated shape because of the use of hollow steel pipes and entire dam was not damaged. The

damaged dam could trap the debris flow up to 5,000 m^3. This effect was indicated in the structural characteristics of the steel pipe, which demonstrated the resilience effect.

7) The result of the current study focused on the combination of the fluid force and the boulder collision force, and, thus, the debris flow has considerably complicated materials. In the near future, several site investigation data will be gathered with regard to the disaster area, and the applicability of the proposed method will be examined regarding debris flow including sediment, driftwood, roots, etc.

References

Adachi, S. (1964). Experimental study on artificial roughness. *Transactions of the Japan Society of Civil Engineers*, *104*, 33-44.

Albaba, A., Lambert, S., Nicot, F., & Chareyre, B. (2015). Modeling the impact of granular flow against an obstacle. In: W, Wu (Ed.), *Recent advances in modeling landslides and debris flows* (pp. 95-105). Switzerland: Springer, Cham.

Armanini, A., Dellagiacoma, F., & Ferrari, L. (1991). From the check dam to the development of functional check dams. In: A. Armanini & G. Didilvio (Eds.). *Fluvial hydraulics of mountain regions* (pp. 332-344). Berlin, Heidelberg: Springer.

Beppu, M., Inoue, R., Ishikawa, N., Hasegawa, Y., & Mizuyama, T. (2011). Numerical simulation of debris flow model by using modified MPS method with solid and liquid particles. *Journal of the Japan Society of Erosion Control Engineering*, *63*(6), 32-42.

Canelas, R.B., Doinguez, J.M., Crespo, A.C., Sliva, M., & Ferreira, R.M. (2015). Debris flow modeling with high-performance meshless methods. In: *Congresso de métodos numéricos em engenharia.* (pp. 1-14). Lisbon: APMTAC.

Daido, A., Yoshizumi, M., & Nakajima, K. (1994). Impact force of mud-debris flows

acting on structure.*Proceedings of Hydraulic Engineering*, *38*, 557-562.

Deymier, C., Tacnet, J-M., & Mathys, N. (1997). Equipements pour l'eau et l'environnement. *Conception et calcul de barrages de correction torrentille*, *CEMAGREF edition.* Retrieved from https://www.quae.com/produit/740/9782853626514/economie-des-equipements-pour-l-eau-et-l-environnement. (*In French*)

Duran J. (1999). *Sables, poudres et grains: introduction á la physique des milieux granulaires*. Paris, France : Eyrolles Sciences. Retrieved from http://jacques-duran.fr/index.php/livres-de-jd/sables-poudres-et-grains. (*In French*)

Ellinas, C., & Walker, A. (1983). Damage on offshore tubular bracing members, *IABSE colloquium, Copenhagen, 1983: Ship collision with bridges and offshore structures,* in co-operation with the Danish Group of IABSE and the Danish Society of Hydraulic Engineering.

Falcetta J. (1985). Un nouveau modèle de calcul de trajectories de blocks rocheus. *Reveue Française de Géomecanique, 30*, 11-17. (*In French*)

Federal Office for the Environment (FOEN). (2016). *Protection against mass movement hazards, guideline for the integrated hazard management of landslides*, *rockfall and hillslope debris flow*. Bern, Switzerland: FOEN.

Hakuno, M. (1997). *Simulation of destruction-destruction using enhancement DEM*, Morikita Publishing Co. Retrieved from https://www.morikita.co.jp/books/book/2342 (*In Japanese*)

Hioki, S., Ote, K., Hiura, K., Okumura, M., & Tomimasu, E. (1973). Studies on mud-flow: Test on distribution of Impact energy. *Journal of Japan Society Civil*

Engineering, *26*(1), 7-16. (*In Japanese*)

Hiramatsu, S., Fukuyama, T., Yamada, T., Onsaka, O., Nakatani, K., Matsumoto, N., Fujimura, N., Kato, N., Shimada, T., Kubo, T., Mutsuo, S., Nishio, Y., & Yoshino, K. (2014). Disaster report on the debris flow occurred on 9 July 2014 in Nagiso, Nagano prefecture. *Journal of Erosion Control Engineering, 67*(4), 38-48.

Hirao, K., Amada, T., Tabata, S., Matsunaga, M., & Ichinose, Y. (1970). An experimental study on impulsive force due to hydraulic bore. *Journal of Japan Society Civil Engineering*, *23*(1), 11-16. (*In Japanese*)

Horiguchi, T., & Katsuki, S. (2015). Analysis of impact load on steel frame check dam using spherical water element DEM. *Japan Society of Civil Engineers, Journal of structural Engineering*, *61*, 912-925.

Horiguchi, T., & Katsuki, S. (2017). DEM analysis on impact load of boulders on open type steel frame dam. *Journal of the Japan Society of Erosion Control Engineering, 70*(3), 51-57.

Horiguchi, T., & Katsuki, S. (2018). Load evaluation of debris flow against steel open sabo dam using DEM, In *Proceedings, INTERPRAENENT 2018 in the Pacific Rim* (pp. 228-235). Toyama, Japan, 1-4 October 2018.

Horiguchi, T., & Komatsu, Y. (2018). Method to evaluate the effect of inclination angle of steel open type check dam on debris flow impact load. *International Journal of Protective Structures, 10*(1)*,* 95-115.

Horiguchi, T., Takahahsi, T., Takamori, K., & Katsuki, S. (2018). Evaluation of load-carrying capacity of full-scale falling protection net using distinct element method. *International Journal of Protective Structures*, *8*(1), 1-20.

Hoshikawa, T., Ishikawa, N., Hikosaka, H., & Abe, S. (1995). Impact response

displacement of fixed steel pipe beam considering local deformation and strain rate effect. *Journal of Japan Society Civil Engineers*, *513*(31), 101-115.

Hübl, J., Nagl, G., Suda, J., & Rudolf-Malklau, F. (2017). Standardized stress model for design of torrential barrier under impact by debris flow (According Austrian Standard Regulation 24801). *International Journal of Erosion Control Engineering*, *10*(1), 47-55.

Hübl, J., Suda, J., Proske, D., Kaitna, R., & Scheidl, C. (2009). Debris flow impact estimation. In *Proceedings, 11th International Symposium on Water Management and Hydraulic Engineering* (pp. 137-148). Ohrid/Macedonia, 1-5 September 2009.

Ikeya, H. (1978). Classification of debris flow. C*ivil Engineering Technical Report, 20*(3)*,* 44-49. (Title is tentatively translated by the authors). (*In Japanese*)

Ishikawa, N., Shima, J., Matsuzawa, R., & Mizuyama, T. (2018). Safety verification of Sabo dams against large scale debris flow. In *Proceedings, INTERPRAENENT 2018 in the Pacific Rim* (pp. 145-152). Toyama, Japan, 1-4 October 2018.

Johnson; R. A. (1989). Retrieval inhibition as an adaptive mechanism in human memory. In H. L. Roediger III & F. I. M. Craik (Eds.), *Varieties of memory & consciousness* (pp. 309-330). Hillsdale, NJ: Erlbaum.

Ministry of Land, Infrastructure Transport and Tourism (MLIT), SABO department. (2018b). Occurrence report sediment disaster due to torrential rain disaster in July 2018 (25th Sep.). Retrieved from http://www.mlit.go.jp/river/sabo/jirei/h30dosha/H30_07gouu_180925.pdf (*In Japanese*)

Ministry of Land, Infrastructure Transport and Tourism (MLIT), SABO department. (2018a). The whole country sediment disaster occurrence report in 2018. Retrieved

from http://www.mlit.go.jp/river/sabo/jirei/h30dosha/h30doshasai.pdf

Misumo, H., Marutan, T., Kaiburi, M., Jitousomo, T., Ohio, H., Shimizu, O., Kubota, T., Ue, H., Kamazawa, A., Kawano, T., Koga, S., Kobayushi, H., Kabuyashi, T., Sakashima, T., Sakatani, Y., Sagara, W., Shimohara, Y., Suzuki, Y., Tukagi, M., Shimada, E., Nakano, K., Fujusawa, Y.n Yamaguchi, K., & Yamada, Y. (2017). Sediment-related disasters by a heavy rainfall in the northern part of Kyushu-Island, Japan in July 2017. *Journal of the Japan Society of Erosion Control Engineering, 70*(4), 31-42.

Miyoshi, I. & Suzuki, M. (1990). Experimental study on impact load on dam due to debris flow. *Journal of the Japan Society of Erosion Control Engineering, 43*(169), 11-19.

Mizuyama T. (2008). Structural countermeasures for debris flow. *International Journal of Erosion Control Engineering*, *1*(2), 38-43.

Mizuyama, T. (1979). Computational method and some consideration on impulsive force of debris flow acting on sabo dam. *Journal of the Japan Society of Erosion Control Engineering, 112*, 40-43.

Mizuyama, T., Shimohigashi, H., Nakanishi, H., & Matsumura, K. (1985). Experiment study of the impact force of debris flow to a Sabo dam made of steel pipes. *Journal of the Japan Society of Erosion Control Engineering*, *37*(136), 30-34.

Mizuyama, T., & Uehara, S. (1984). Observed data of the depth and velocity of debris flow. *Journal of the Japan Society of Erosion Control Engineering*, 37(4), 23-26.

Mizuyama, T. & Senoo, K. (1984). Flood traveling time in small mountain basins and rainfall intensity in short duration. *Journal of the Japan Society of Erosion Control Engineering*, *37*(4), 20-22.

National Institute for Land and Infrastructure Management (NILIM), Ministry of Land, Infrastructure and Transport. (2016a). *Manual of technical standard for establishing sabo plan for debris flow and driftwood* (Technical Note of National Institute for Land and Infrastructure Management No. 904). Retrieved from http://www.nilim.go.jp/lab/bcg/siryou/tnn/tnn0904pdf/ks0904.pdf

National Institute for Land and Infrastructure Management (NILIM), Ministry of Land, Infrastructure and Transport. (2016b). *Manual of technical standard for designing sabo facilities against debris flow and driftwood* (Technical Note of National Institute for Land and Infrastructure Management No. 905). Retrieved from http://www.nilim.go.jp/lab/bcg/siryou/tnn/tnn0905pdf/ks0905.pdf /

Osaka, T., Mizuyama, T., Takahashi, E., Kunitomo, M., Ishizuka, T., Utunomiya, R., & Yokoyama, K. (2013). Field observations of unit weight of flowing debris flows by force plate in Sakurajima, Japan. *Journal of the Japan Society of Erosion Control Engineering, 65*(6), 46-50.

Ou, G., Kobashi, S., & Mizuyama, T. (1991). Prediction of debris flow peak discharge by statistical methods. *Journal of the Japan Society of Erosion Control Engineering, 44*(4), 24-29.

Richefeu, V., & Villard, P. (2016). *Modeling gravity hazards from rockfalls to landslides*. UK: ISTE press and Elsevier.

Rimbock, A. (2004). Design of rope net barriers for woody debris entrapment. In *Proceedings*, *INTERPRAEVENT 2004* (pp. 265-276). Riva del Garda, 26th May 2004.

Suzuki, T., & Hotta, N. (2016). Development of modified particles method for simulation of debris flow using constitutive equations. *International Journal of*

Erosion Control Engineering, 9(4), 165-173.

Sonoda, Y., Tsuchiya, Y., Tamai, H., & Shima, J. (2016). A fundamental study on the load carrying capacity of steel frame check dam. *Japan Society of Civil Engineers, Journal of Structural Engineering, A, 62*, 1019-1030.

Takahashi, T. (2004). The occurrence and flow mechanism and measurement of debris flow. In Takahashi, T. (Ed.), *New Field Science Series*. Aichi, Japan: Kinmiraisya company. Retrieved from http://www.kinmiraisha.com/-19-doseki.htm (*In Japanese*)

Yamamoto, R., & Toyota, M. (2016). Analytical study of the debris flow occurred in July, 2014 in Nagiso town, Nagano prefecture. *Journal of Japan Society of Civil Engineers Series F6 (Safety Problem), 72*(2), 139-144.

Fig. 1. Photographs of sabo dams. (a) An example of open sabo dam made of steel-tubes which is located in Hyogo, Fukuchi River, Japan. The sabo dam maintains a continuous river. (b) Same kind of open sabo dam where the downstream part of the structure has been filled in by a boulder laden debris flow; some trapped boulders are still visible, and an idea of the dimensions can be made in comparison with the standing man at the bottom left of the photograph.

Fig. 2. Overview of Nagiso-cho, Kisodake disaster map of investigation points from ① to ⑨ for boulder grading sizes. The concerned zone is about 2.0 km in length. The boulder-size investigation was made from 200 randomly selected boulders within a distance of 200 m before and after each sabo dam (Shima et al., 2015). The squares are the small check dams. The small secondary check dam is the location where the peak discharge of the debris flow has been deemed to occur.

Fig. 3. Measured elevation and horizontal distance from the sabo dam is shown at the first Nashizwa sabo dam. The curved line represents the trapped volume of boulders and the straight line represents the volume as it was planned. The average riverbed slope is 11.3°, and the riverbed possesses a straight channel for a distance of about 200 m downstream of the sado dam.

Fig. 4. A boulder size investigation result: the extracted data is the number of boulders, the grading of sizes, and some percentiles.

Fig. 5. Review of damage mechanism. (a) The boulder laden debris flow first hit the sabo dam, (b) the debris flow caused damage in the vicinity of the crest, (c) the boulder made the rear steel pipe collapse, (d) the pipe of the crest outflowed in the river, (e) the major boulder laden debris flow directly hit the rear steel pipe, and (f) 50% of the sabo dam was broken, and the structural member outflowed into the Kiso River.

Fig. 6. Diagram of screwed flange. (a) Initial condition of flange and bolts, and (b) deformed condition against moment direction.

Fig. 7. Axial-stress distribution diagram.

Fig. 8. Flow chart of the partial section method.

Fig. 9. Model of flange and bolts. (a) Axial force and strain (ε) relation, and (b) moment force and curvature (φ) relation: the solid line represents the value obtained from the calculations, and the dashed line is the approximation.

Fig. 10. Calibration of the parameters involved in Ellinas equation.

Fig. 11. An overview of the damage caused on the tubular junctions. (a) All secondary structural members shown after the debris flow disaster, and (b) a connection tube is largely deformed due to the debris flow.

Fig. 12. Scheme of the analysis model: the roughness model is based on Japanese sabo dam design.

Fig. 13. The first Nashizawa sabo dam model and design. (a) Lateral view showing the lower and upper connections, (b) front view, (c) sketch with sizes, and (d) the employed model is indicated in each member. The front part has 7 vertical members, and the steel pipe thickness is 22 mm. The secondary part has 4 vertical members. Another member's thickness is 12.7 mm. The member density is defined thanks to a Monte-Carlo method.

Fig. 14. Reproduction analysis: (a) $t = t_0$ s, (b) $t = t_0 + 2$ s, (c) $t = t_0 + 7$ s, and the first component is generated at the time the front part is broken. (d) $t = t_0 + 11.3$ s, the time of maximum

impulsive load. (e) $t = t_0 + 14.5$ s, and (f) $t = t_0 + 16$ s.

Fig. 15. Reinforced analysis. (a) $t = t_0$ s, (b) $t = t_0 + 2$ s, (c) $t = t_0 + 7$ s, (d) $t = t_0 + 11.3$ s, (e) $t = t_0 + 14.5$ s (f) $t = t_0 + 16$ s.

Fig. 16. Load-carrying performance of reproduction analysis compared with the reinforced analysis: (a) the sum of forces on the lower members, and (b) the sum of forces on the upper member.

Fig. 17. The proposed method expressed damage circumstance: (a) the coupling joint part was first broken in the structure ($t = t_0 + 10$ s). The coupling joint was separated due to boulder impact, (b) the secondary member is largely deformed ($t = t_0 + 11.3$ s). The dent deformation reached about 95% of the tube diameter.

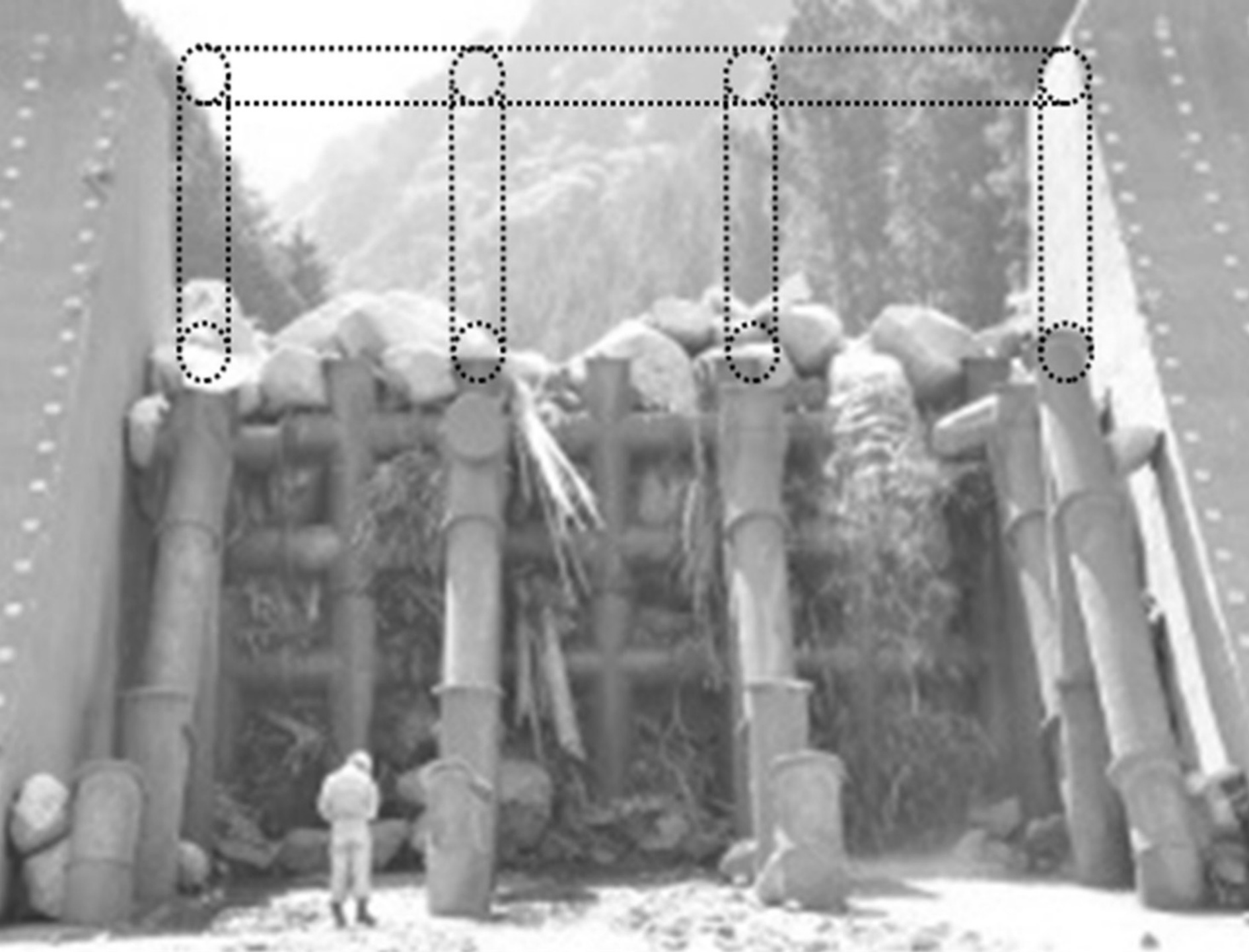

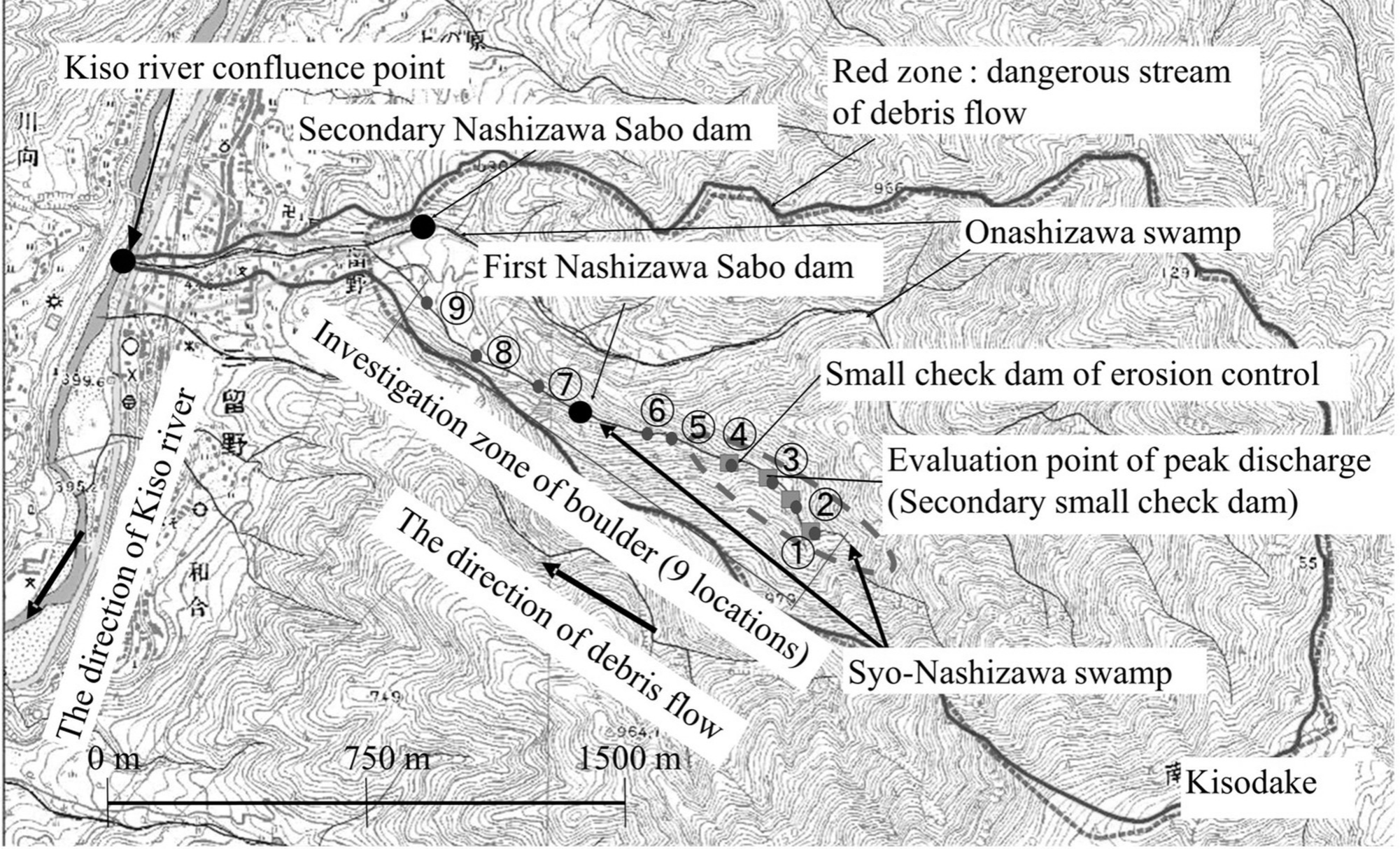
Kiso river confluence point
Secondary Nashizawa Sabo dam
Red zone : dangerous stream of debris flow
Onashizawa swamp
First Nashizawa Sabo dam
⑨
⑧
⑦
⑥
⑤
④
③
②
①
Small check dam of erosion control
Investigation zone of boulder (9 locations)
Evaluation point of peak discharge (Secondary small check dam)
The direction of Kiso river
The direction of debris flow
Syo-Nashizawa swamp
0 m
750 m
1500 m
Kisodake

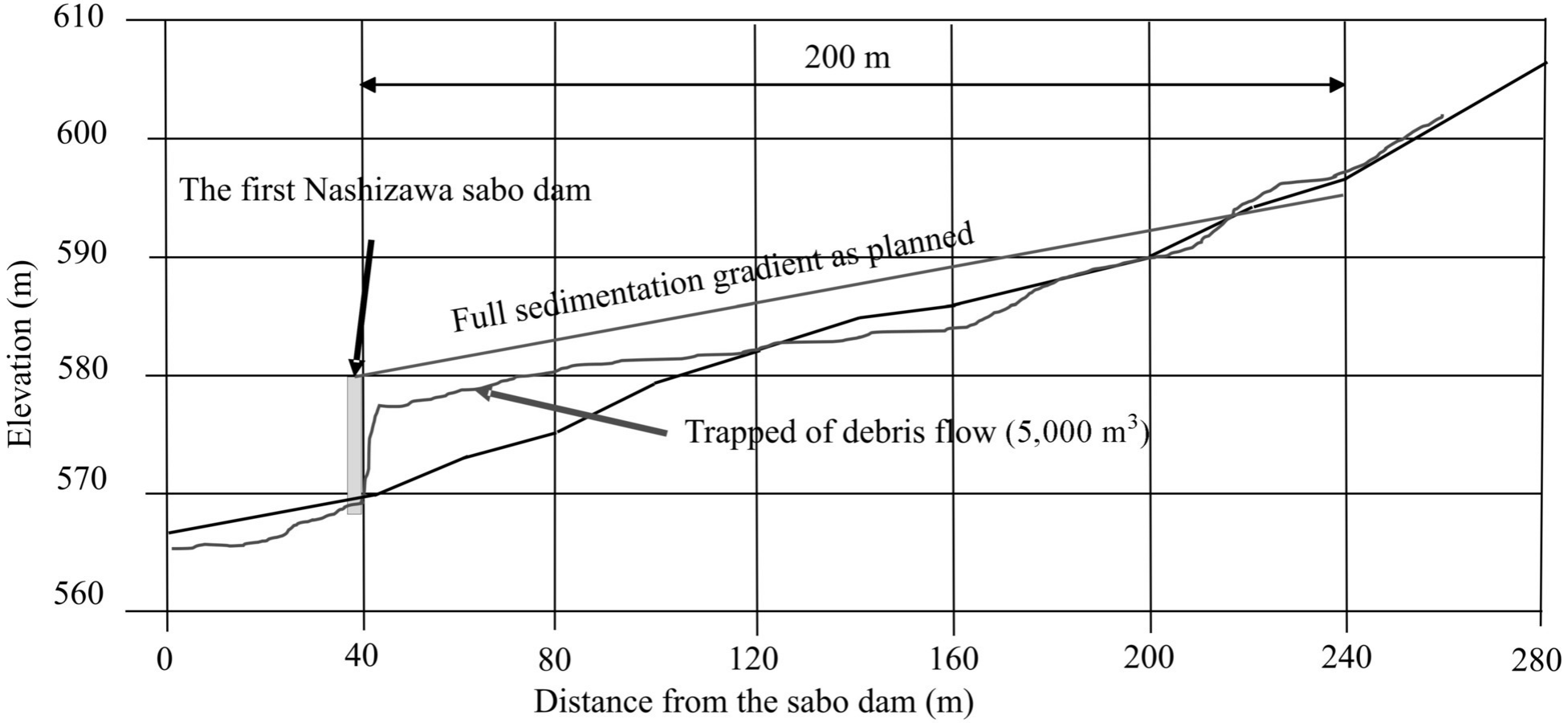
610
600
590
580
570
560
Elevation (m)
200 m
The first Nashizawa sabo dam
Full sedimentation gradient as planned
Trapped of debris flow (5,000 m3)
0
40
80
120
160
200
240
280
Distance from the sabo dam (m)

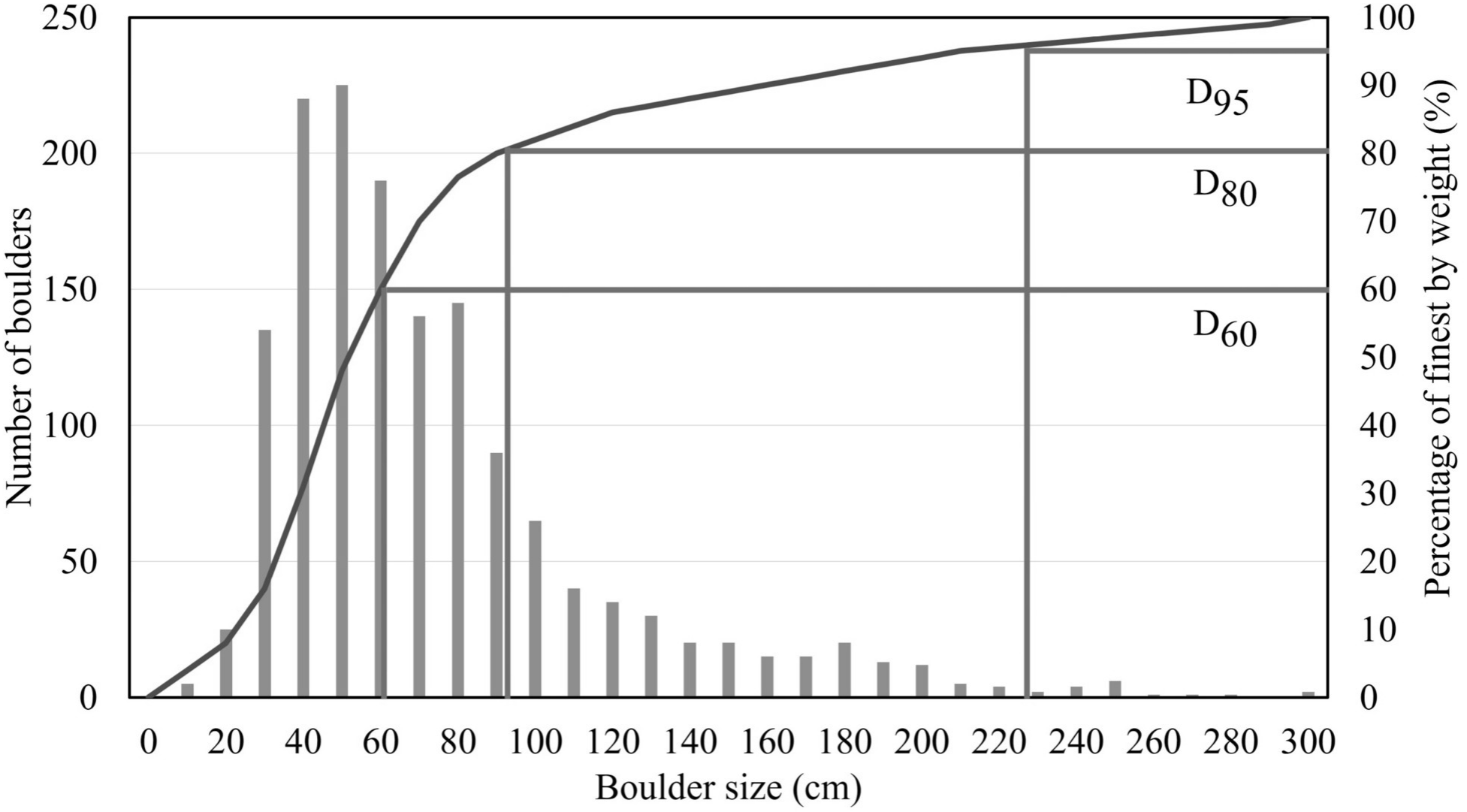
250
200
150
100
50
0
Number of boulders
100
90
80
70
60
50
40
30
20
10
0
Percentage of finest by weight (%)
D95
D80
D60
0
20
40
60
80
100
120
140
160
180
200
220
240
260
280
300
Boulder size (cm)

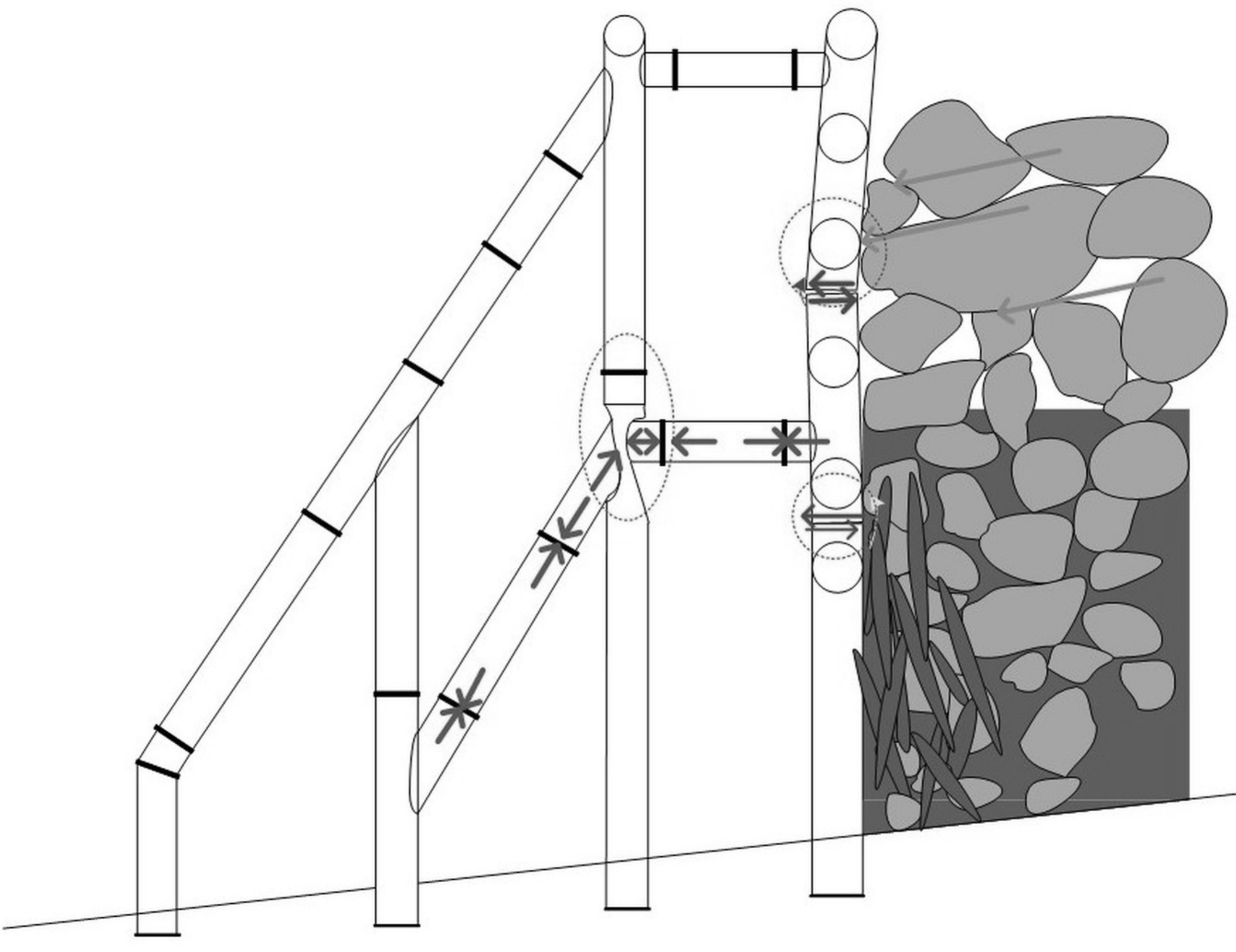

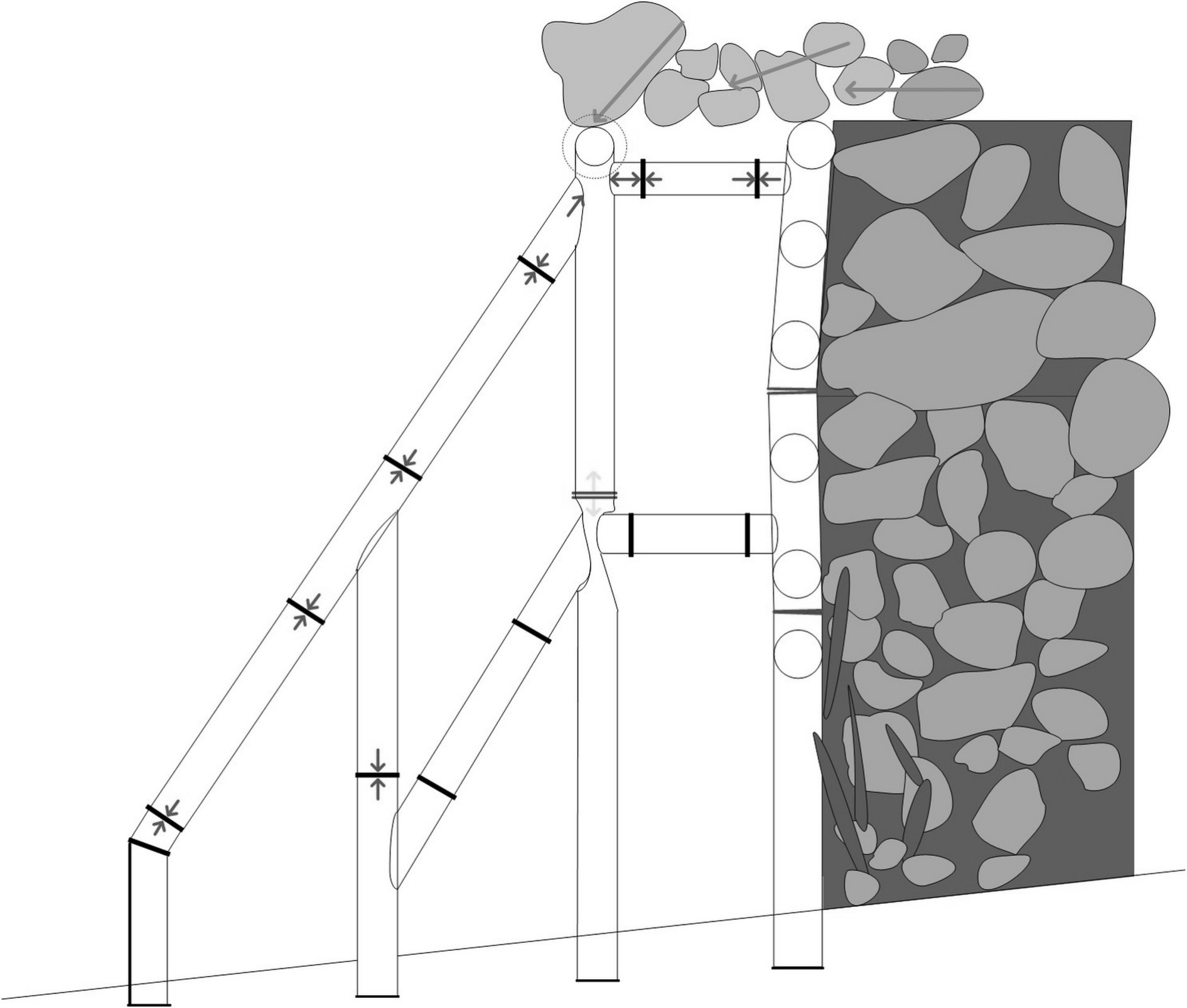

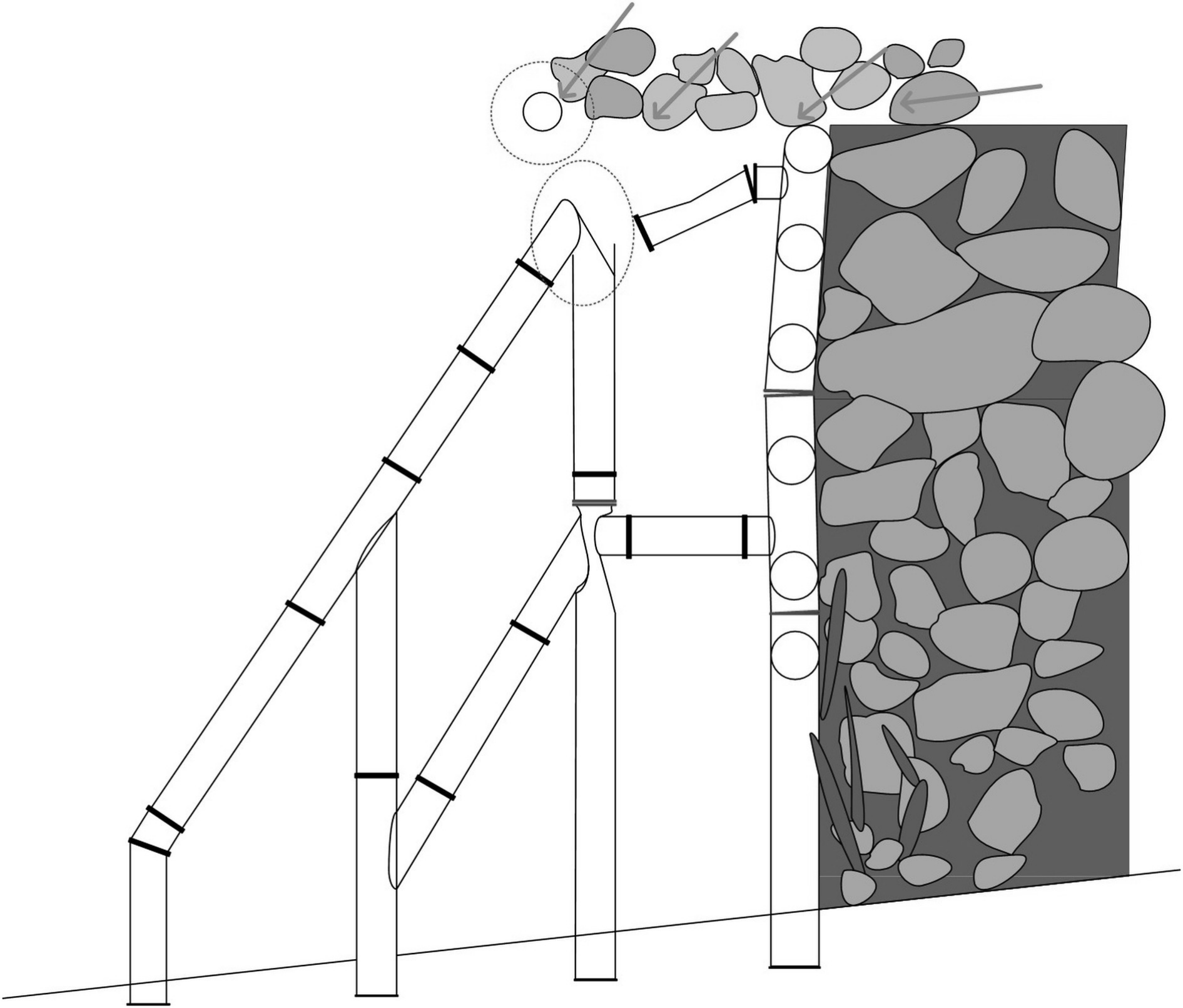

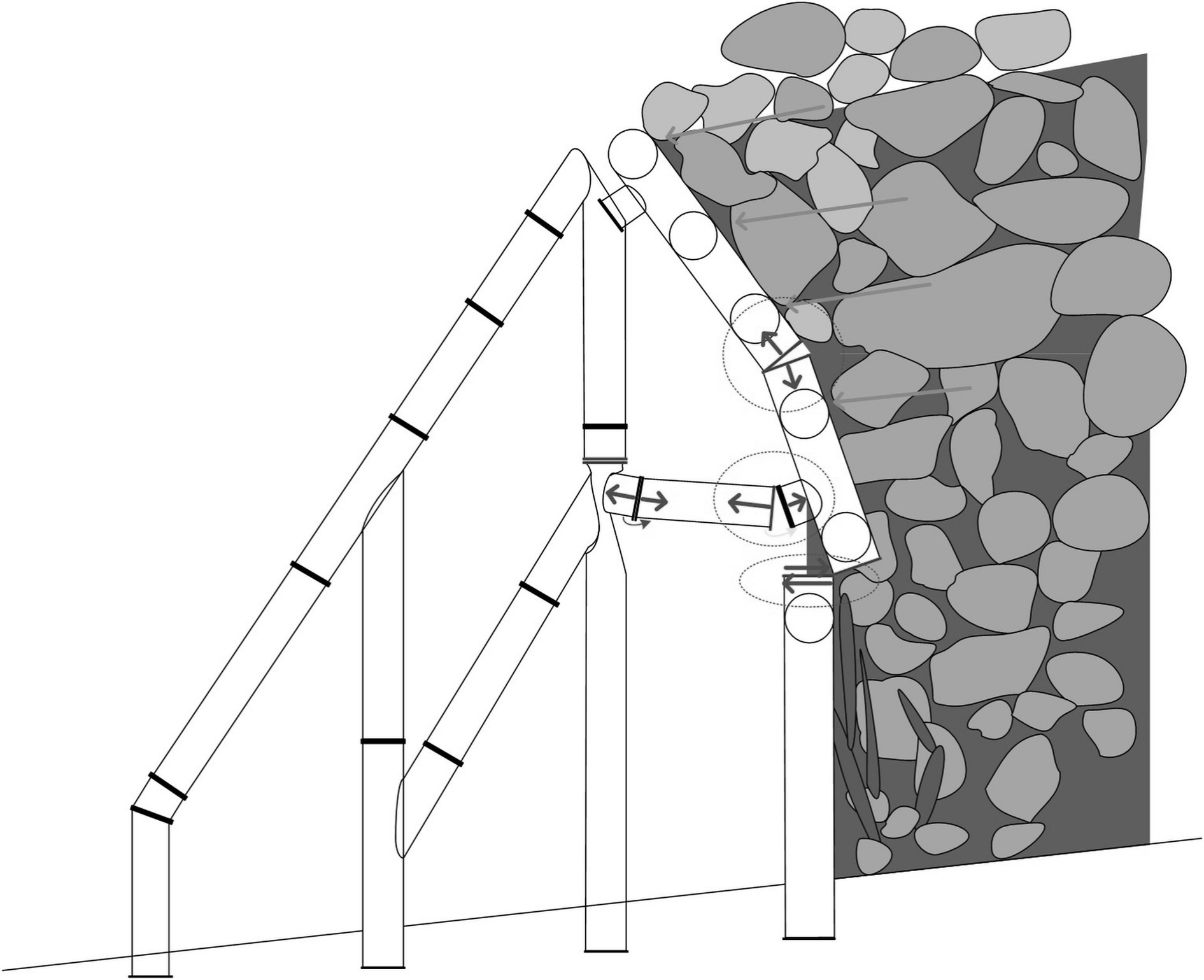

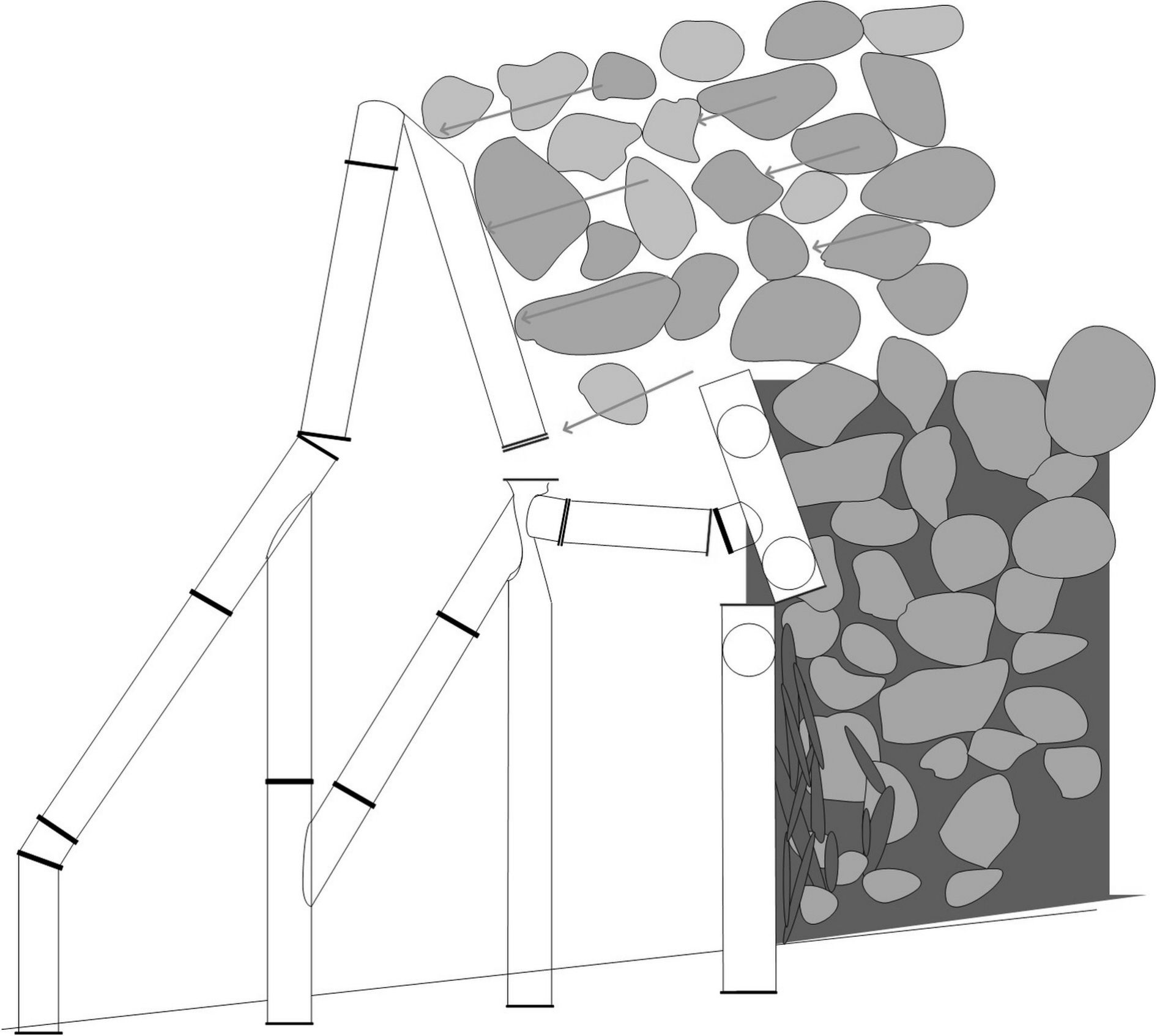

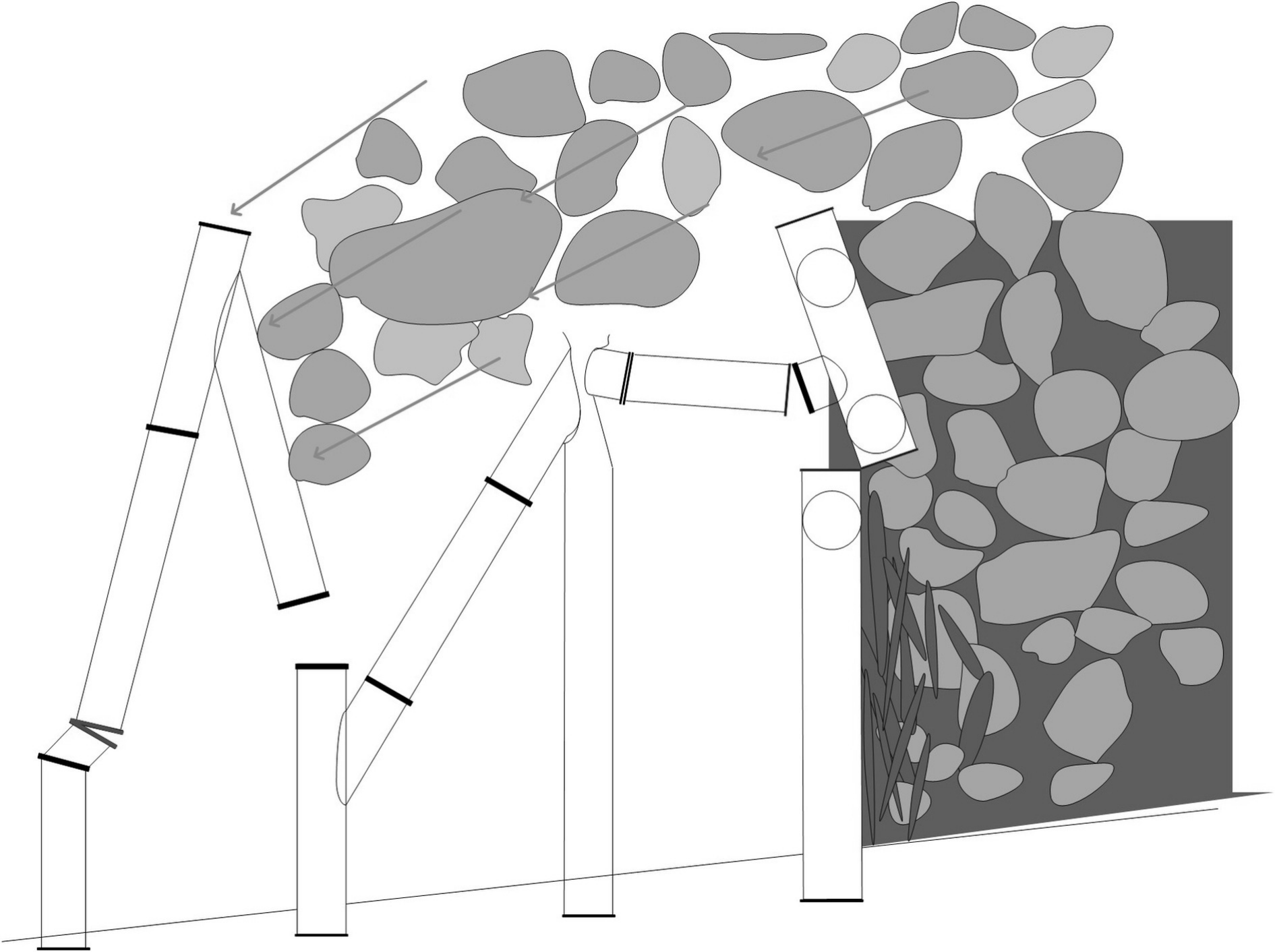

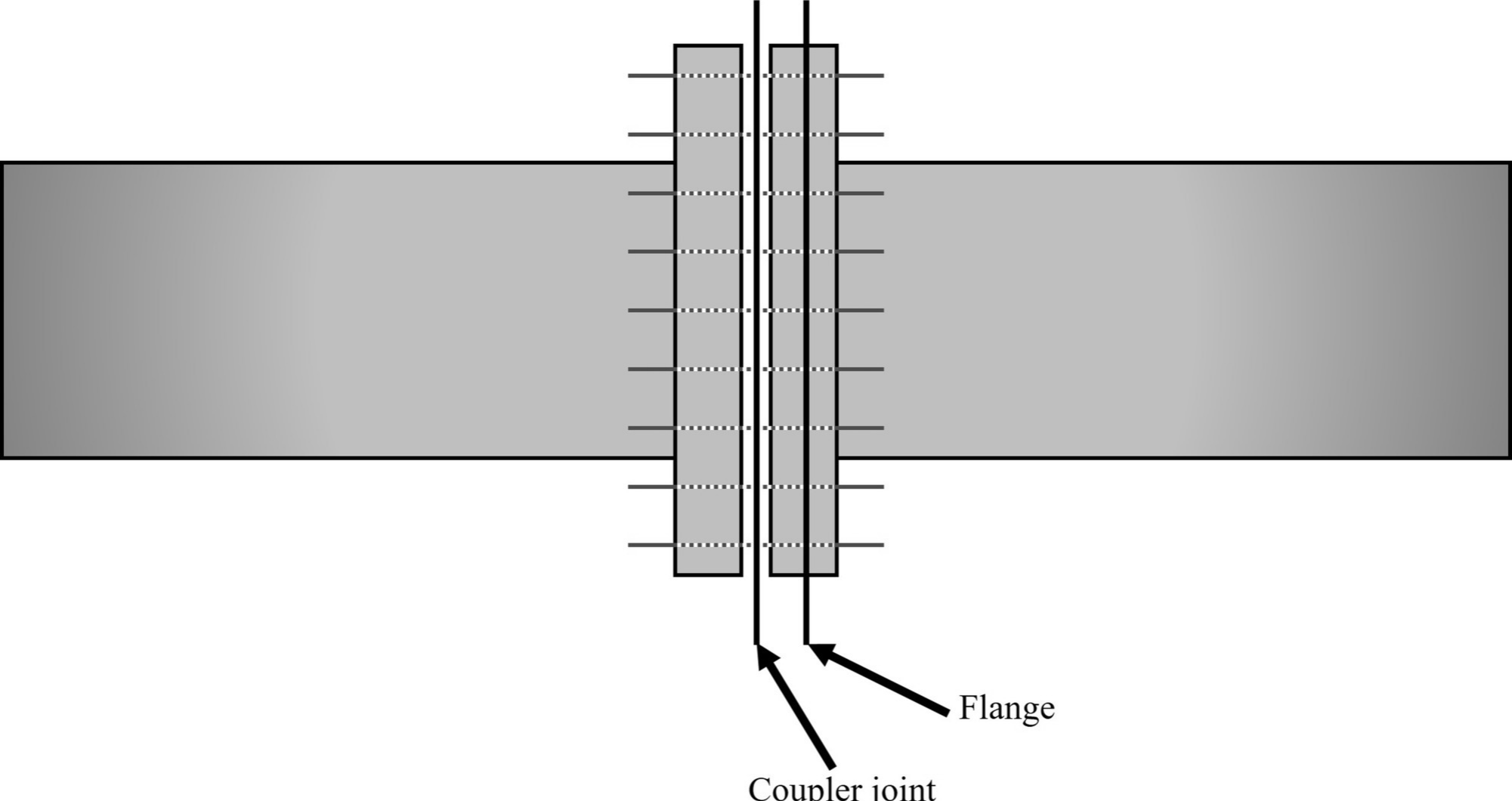
Flange
Coupler joint

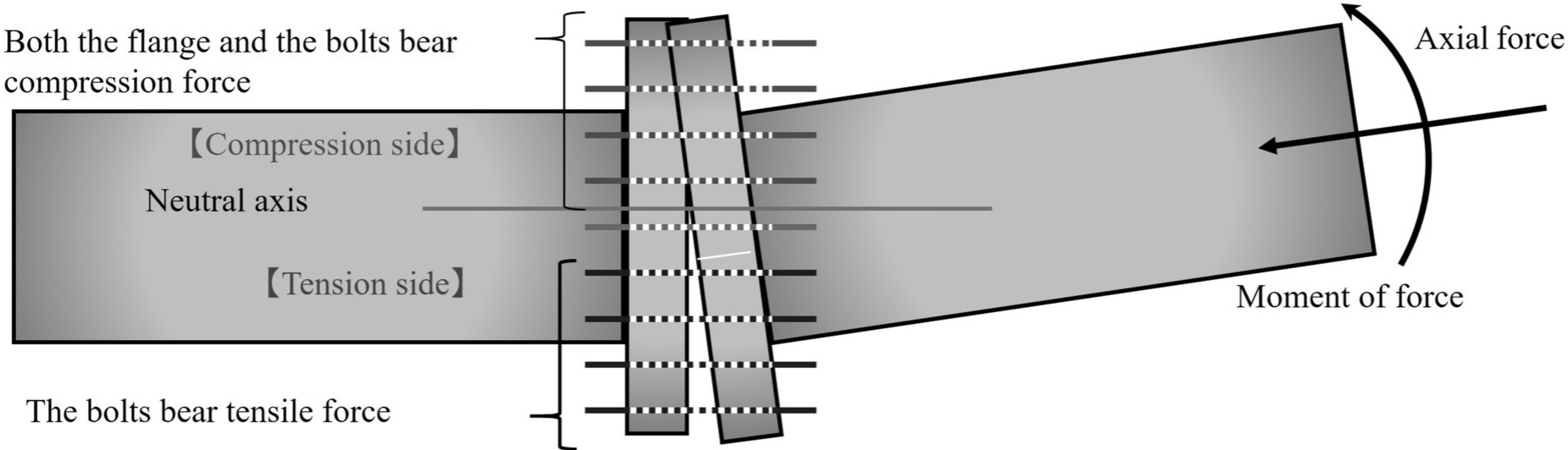
Both the flange and the bolts bear compression force
【Compression side】
Neutral axis
【Tension side】
The bolts bear tensile force
Axial force
Moment of force

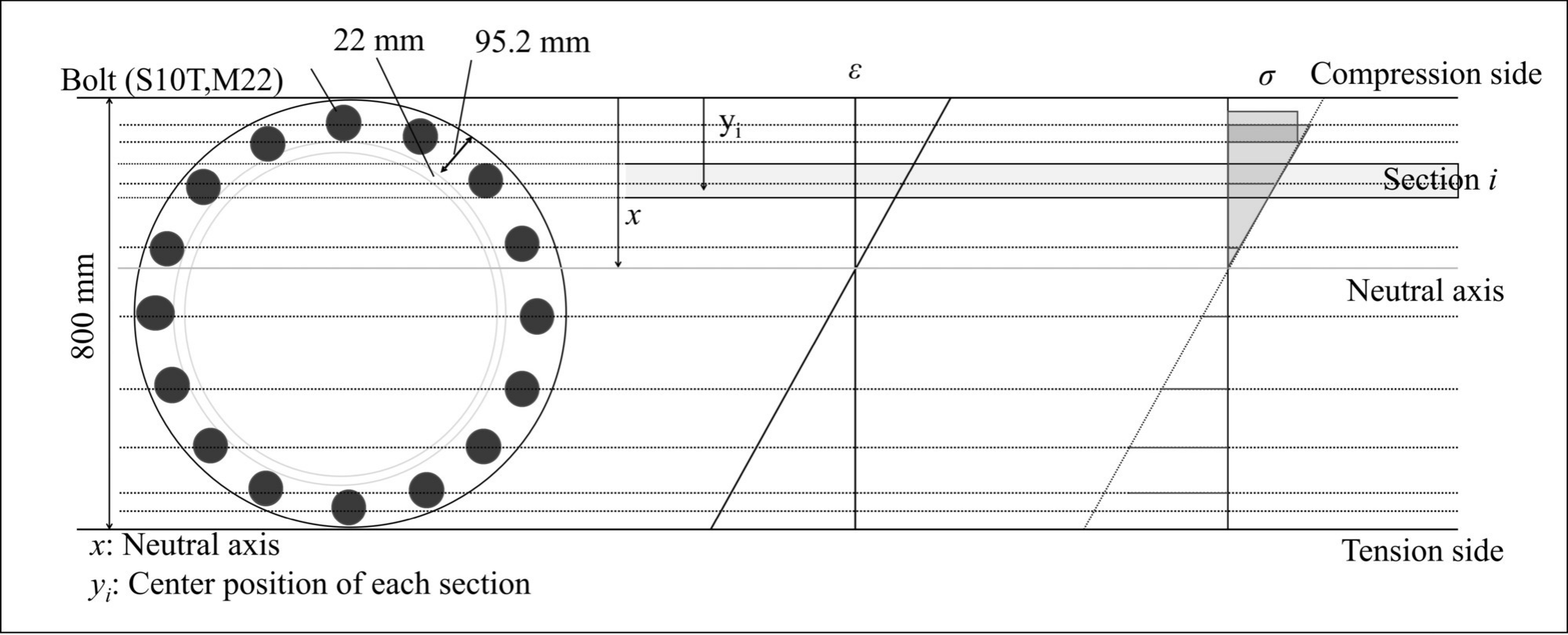

The schematic chart of strain and stress （ Bernoulli-Euler hypothesis ）

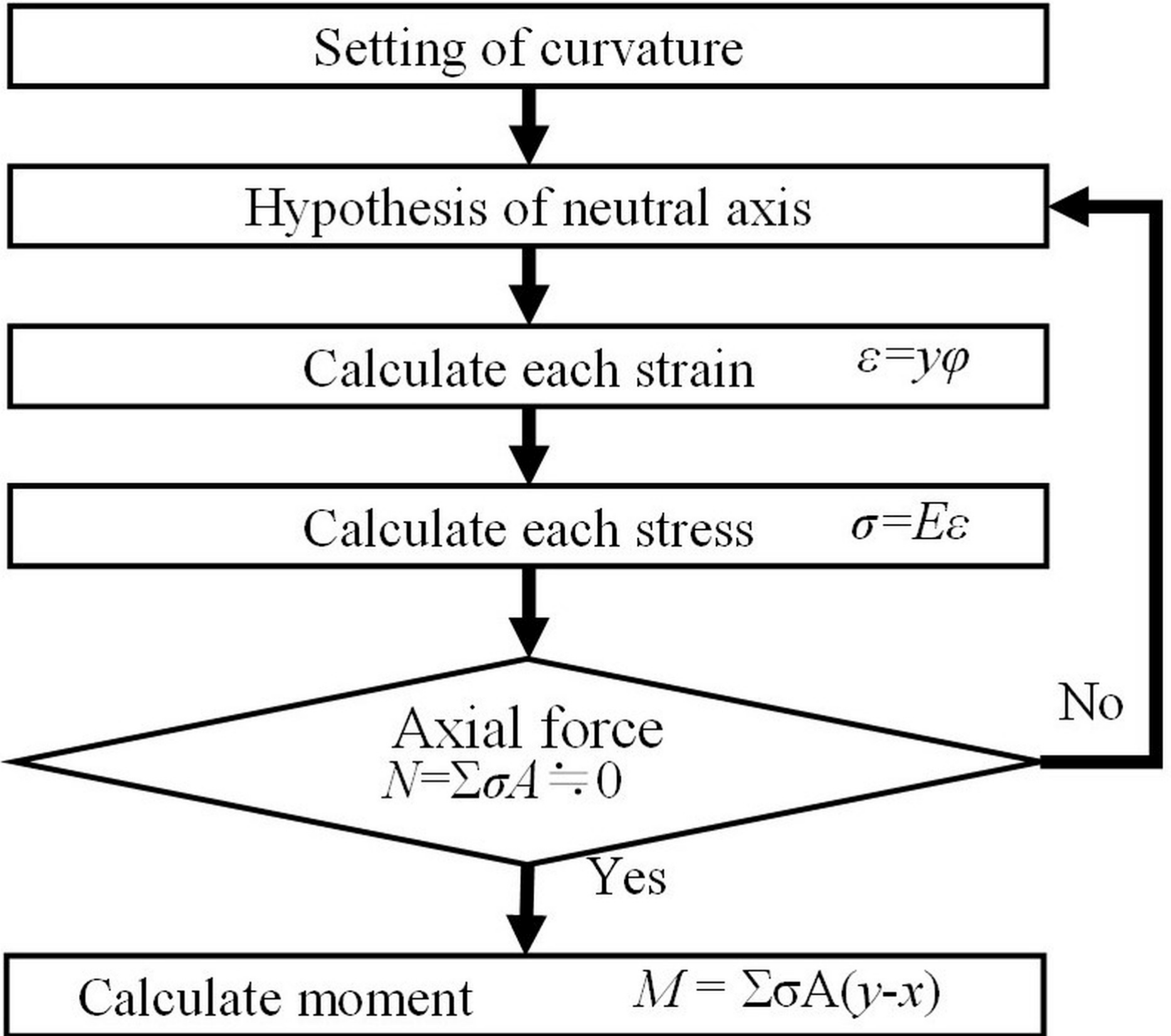
Setting of curvature
Hypothesis of neutral axis
Calculate each strain
$\varepsilon = y\varphi$
Calculate each stress
$\sigma = E\varepsilon$
Axial force
$N = \Sigma\sigma A \fallingdotseq 0$
No
Yes
Calculate moment
$M = \Sigma\sigma A(y\text{-}x)$

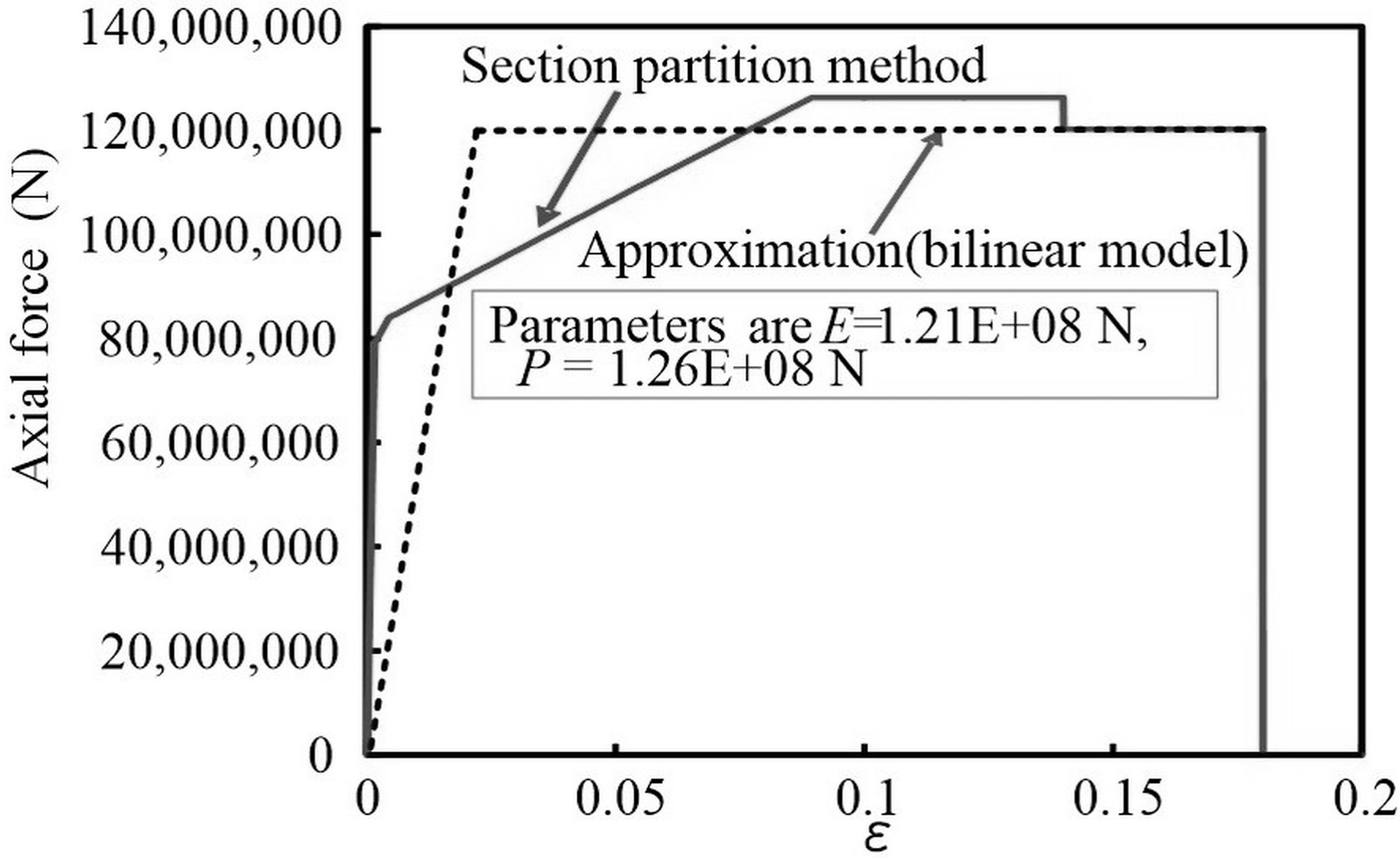
140,000,000
120,000,000
100,000,000
80,000,000
60,000,000
40,000,000
20,000,000
0
Axial force (N)
Section partition method
Approximation(bilinear model)
Parameters are E=1.21E+08 N,
P = 1.26E+08 N
0
0.05
0.1
0.15
0.2
ε

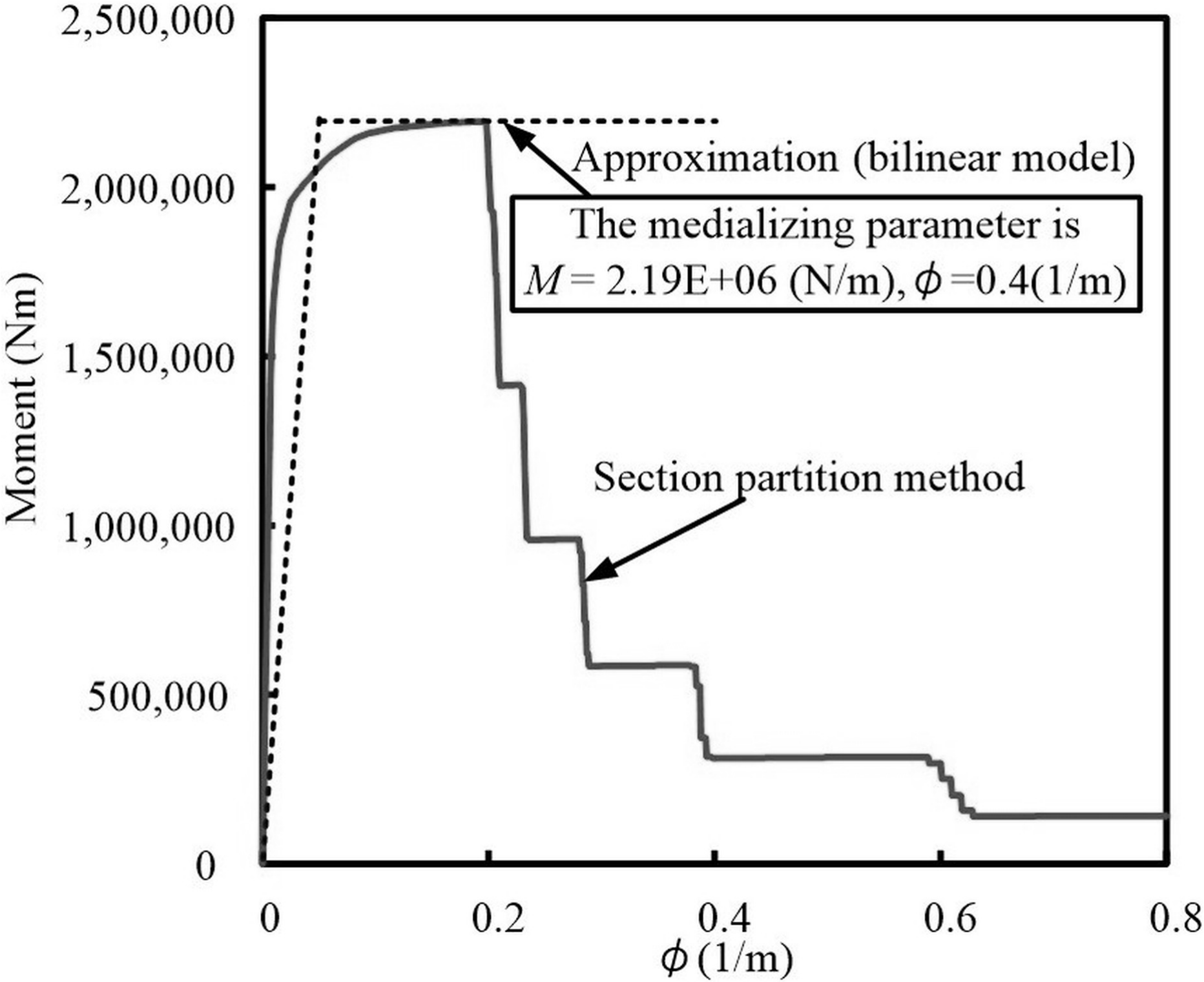
2,500,000
2,000,000
1,500,000
1,000,000
500,000
0
Moment (Nm)
0
0.2
0.4
0.6
0.8
ϕ (1/m)
Approximation (bilinear model)
The medializing parameter is
M = 2.19E+06 (N/m), ϕ =0.4(1/m)
Section partition method

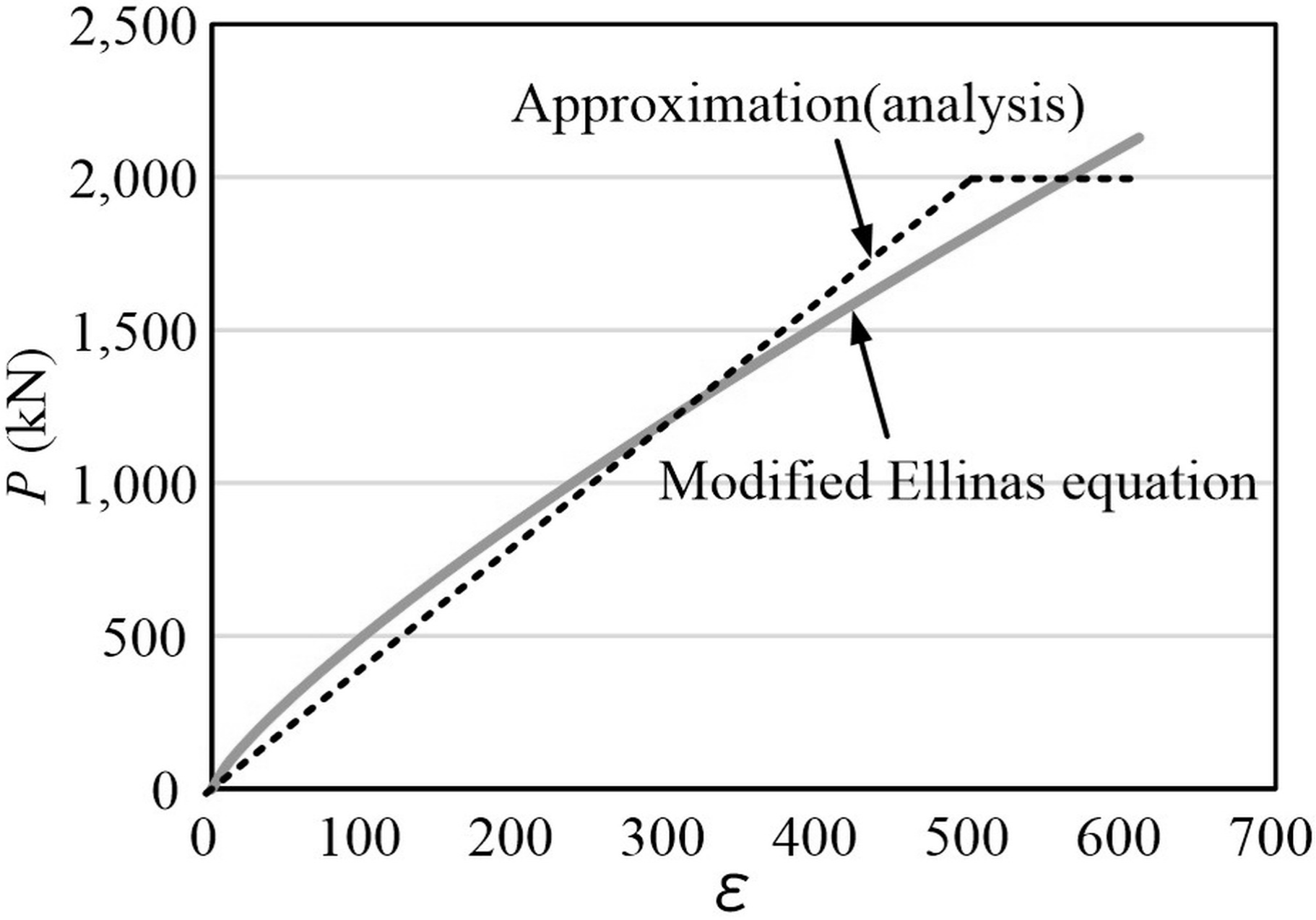
2,500
2,000
1,500
1,000
500
0
P (kN)
0
100
200
300
400
500
600
700
ε
Approximation(analysis)
Modified Ellinas equation

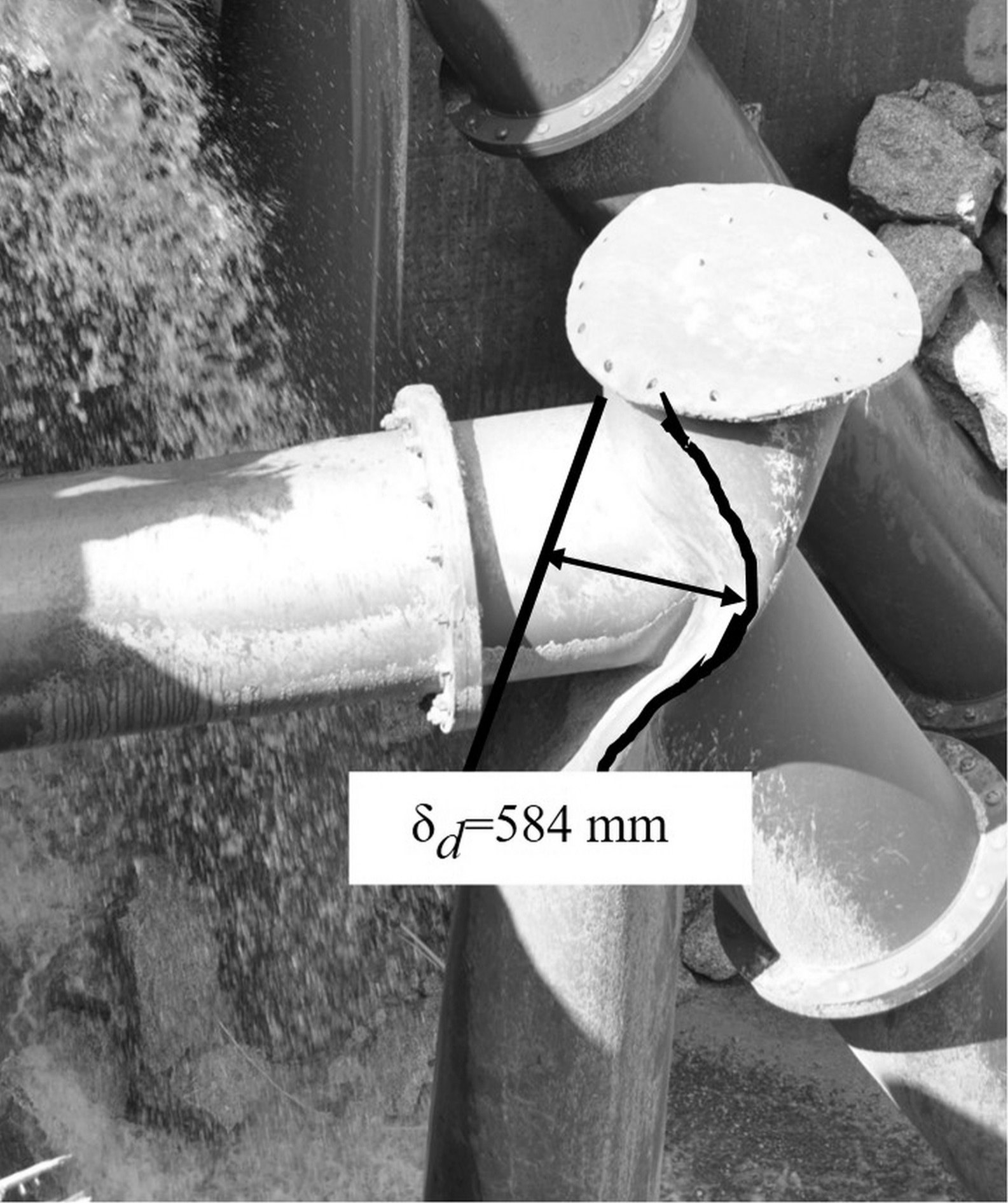
δ_d=584 mm

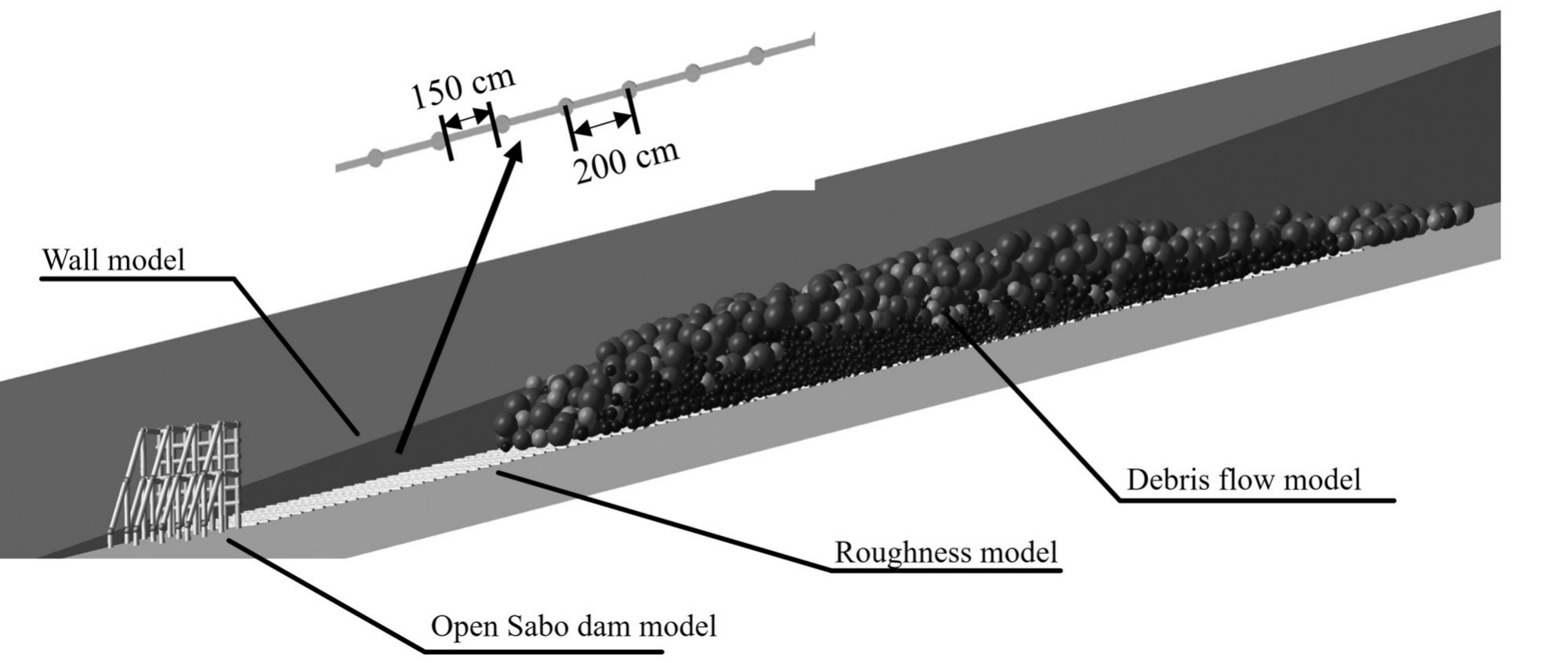
150 cm
200 cm
Wall model
Debris flow model
Roughness model
Open Sabo dam model

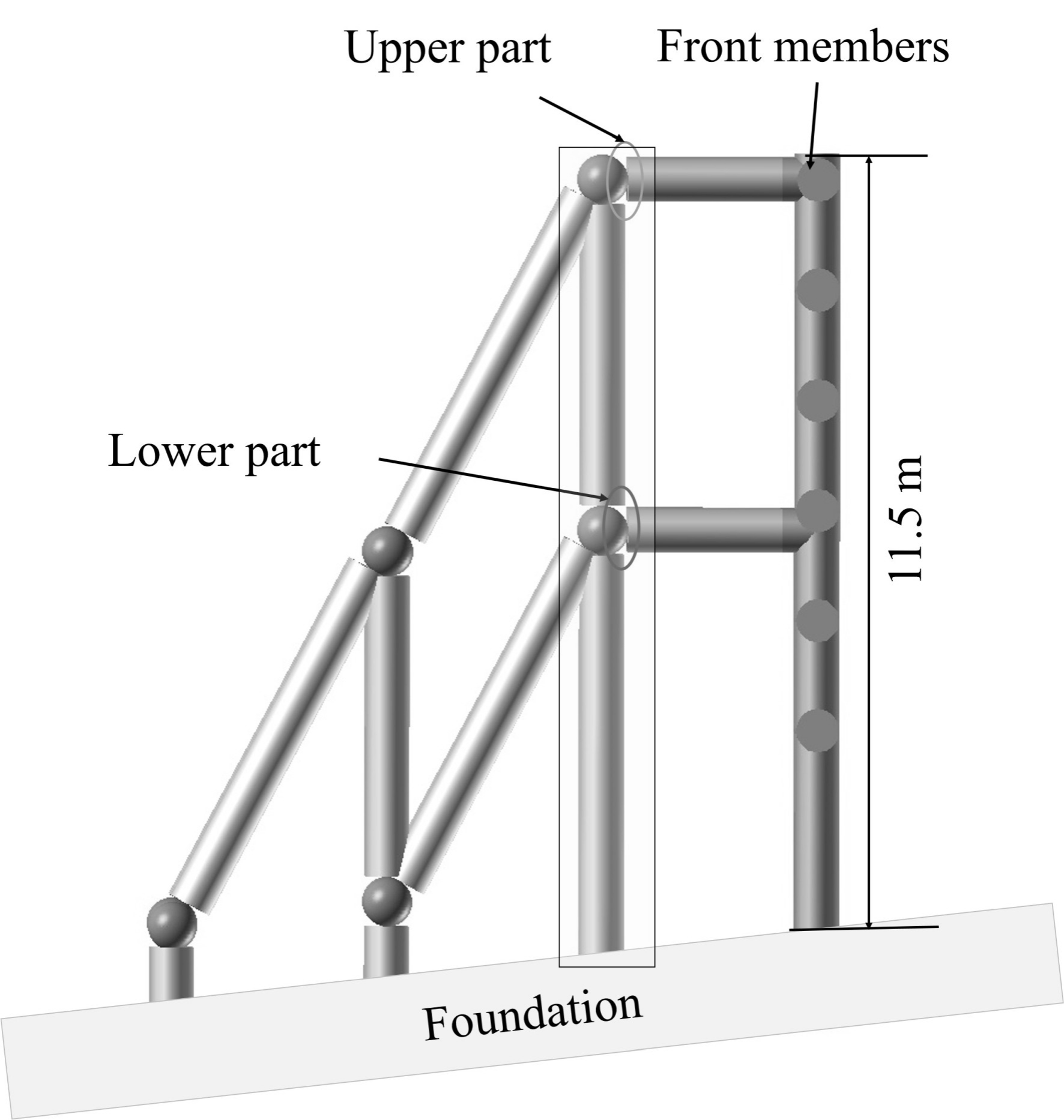
Upper part
Front members
Lower part
11.5 m
Foundation

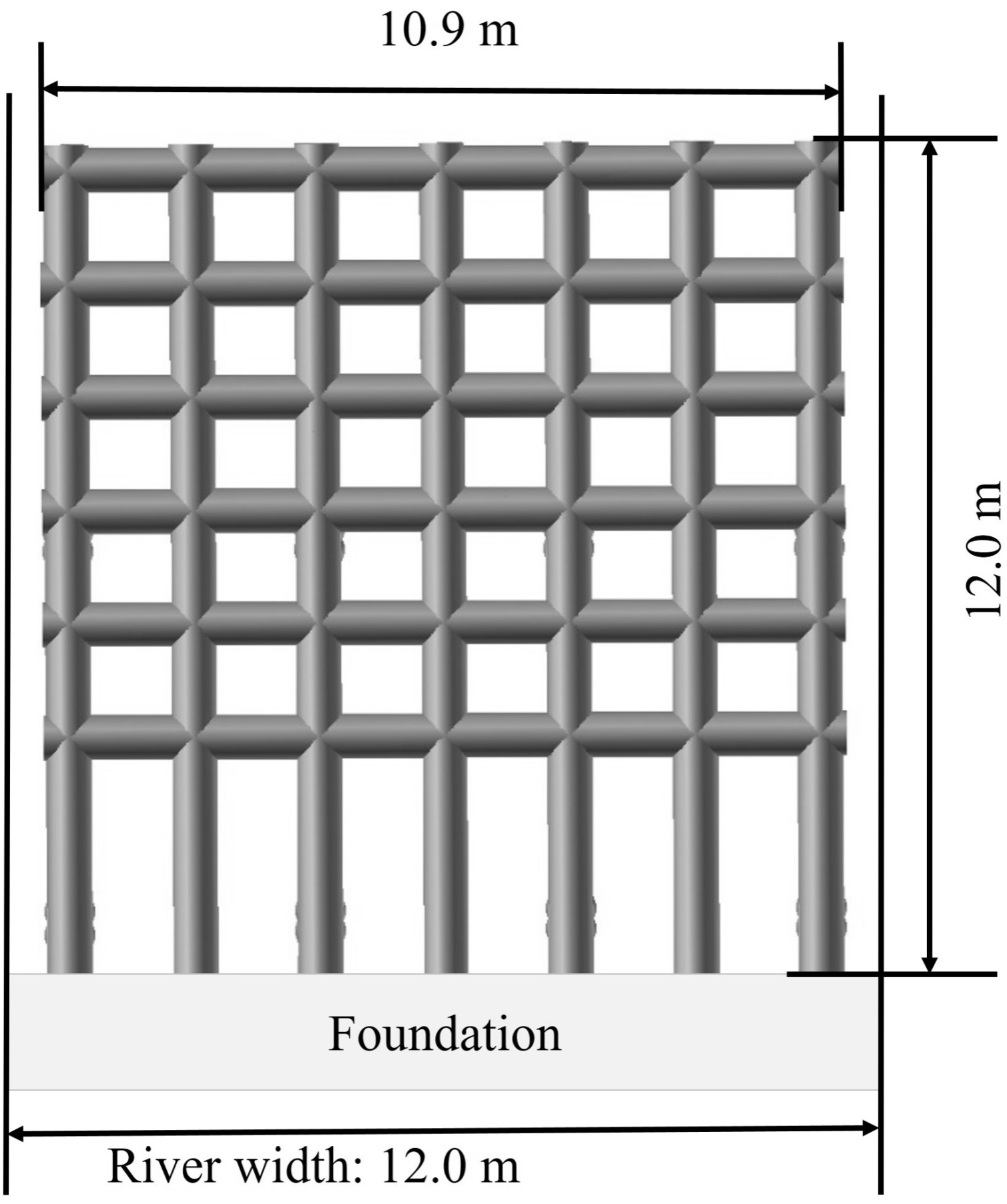
10.9 m
12.0 m
Foundation
River width: 12.0 m

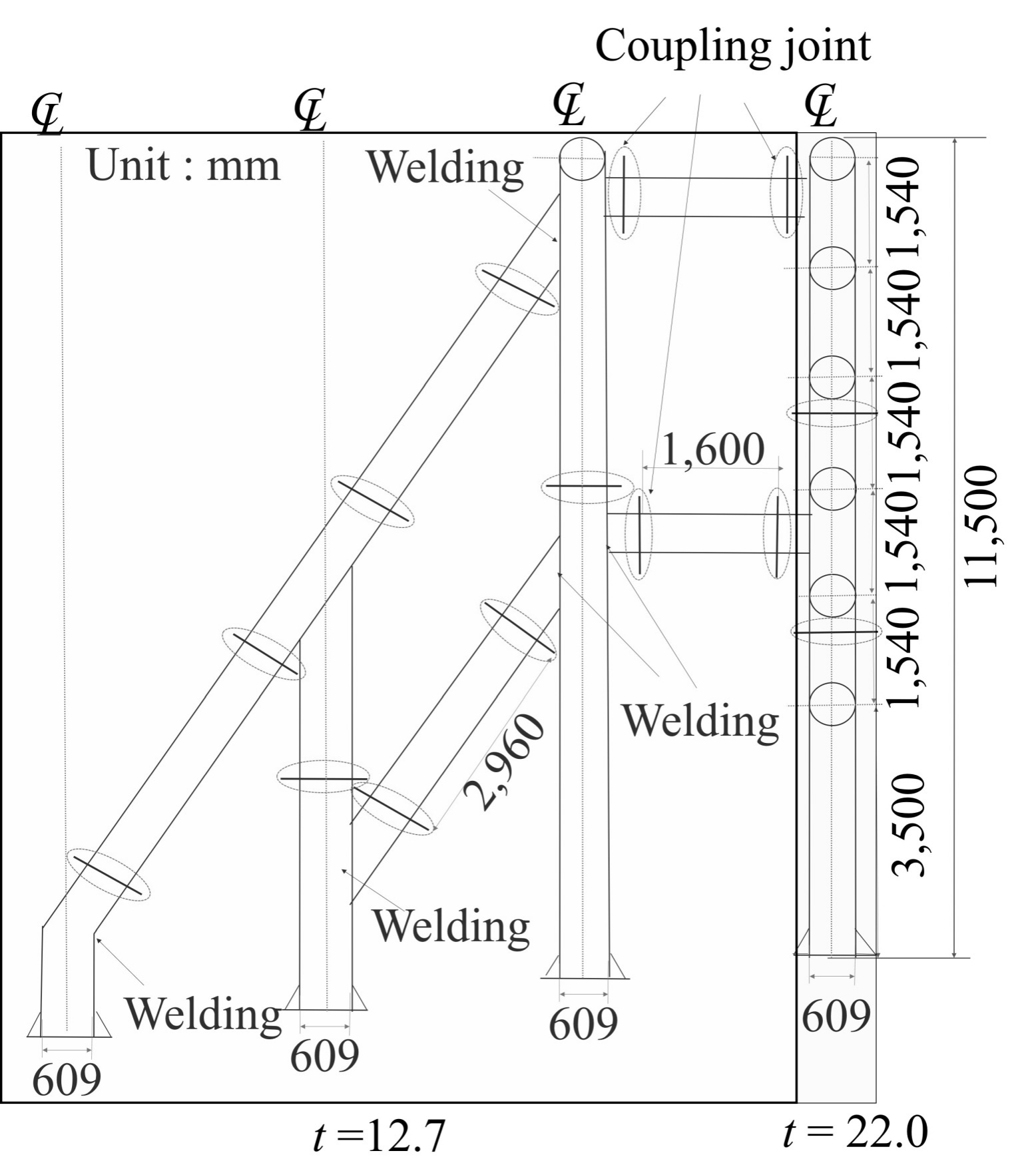

t =12.7 t = 22.0

t : Unit of steel pipe thickness (mm)

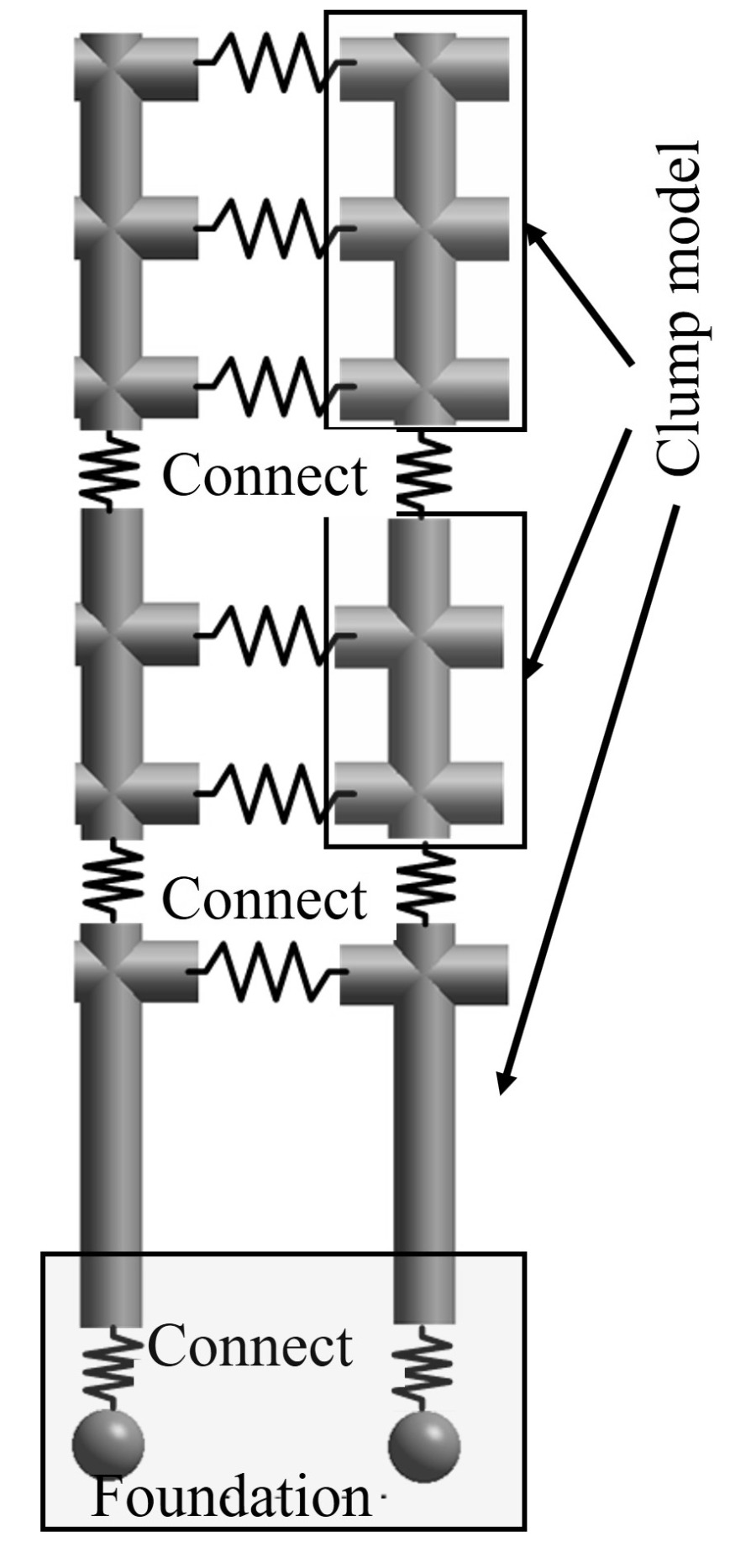
Clump model
Connect
Connect
Connect
Foundation

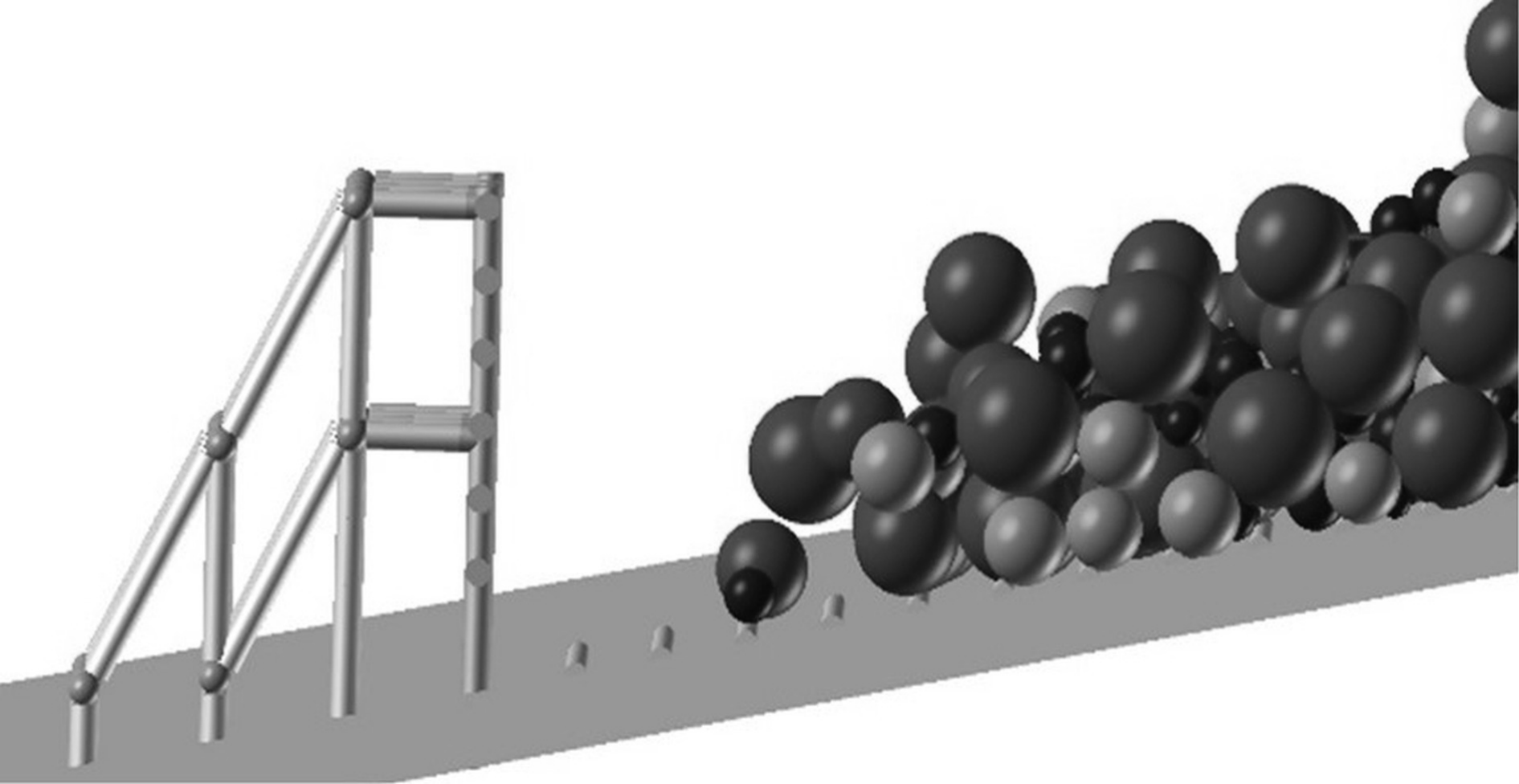

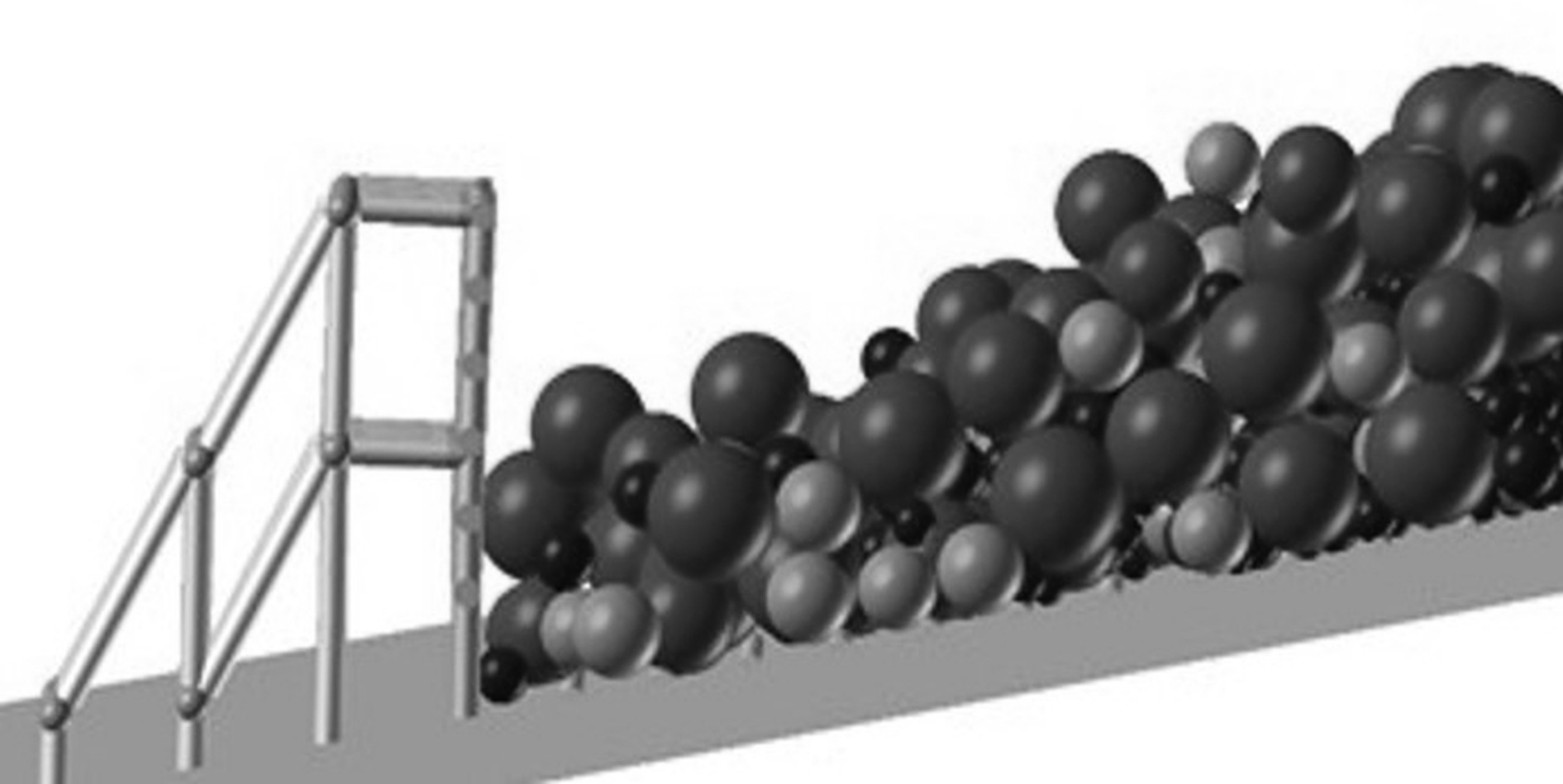

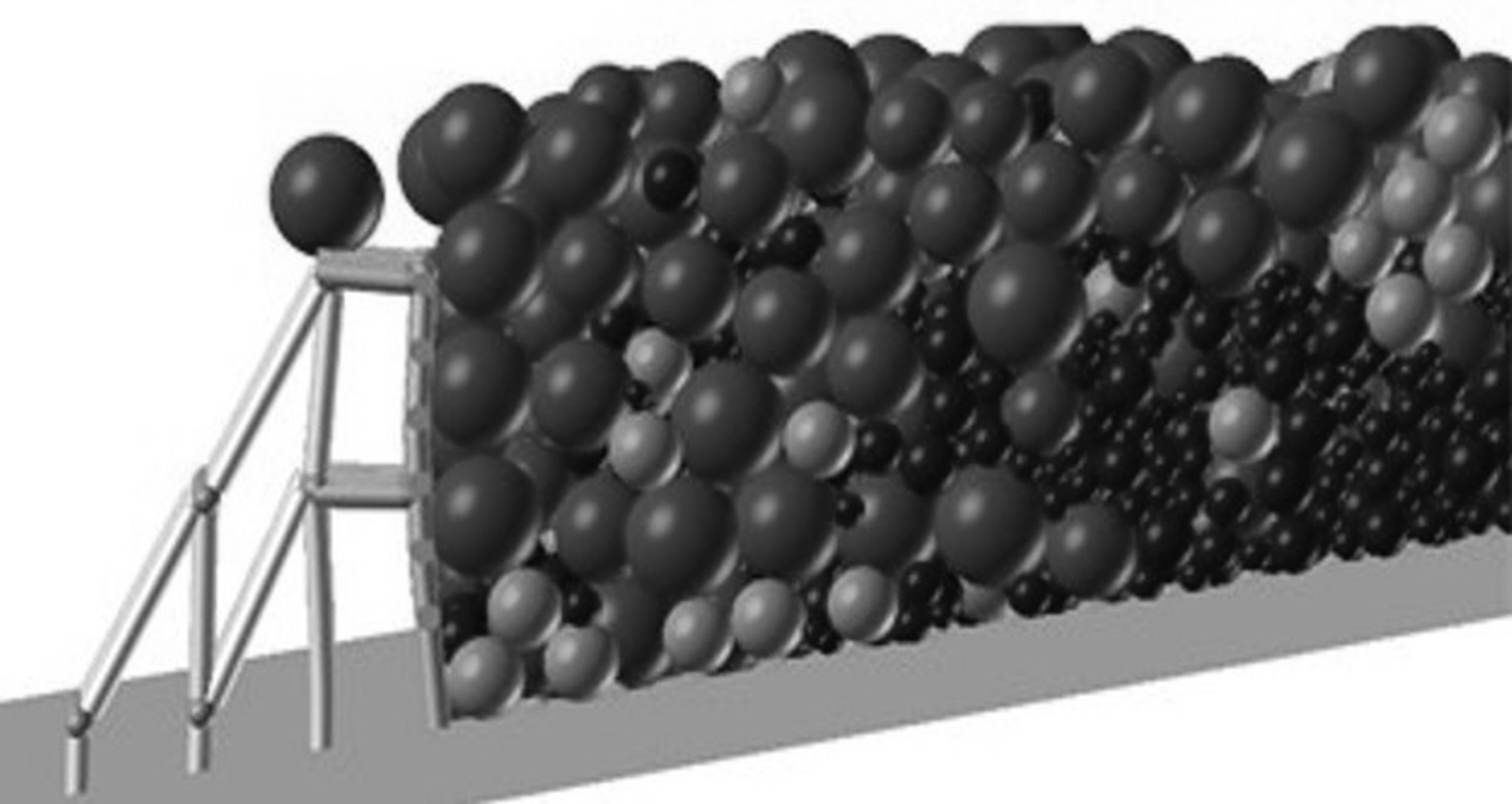

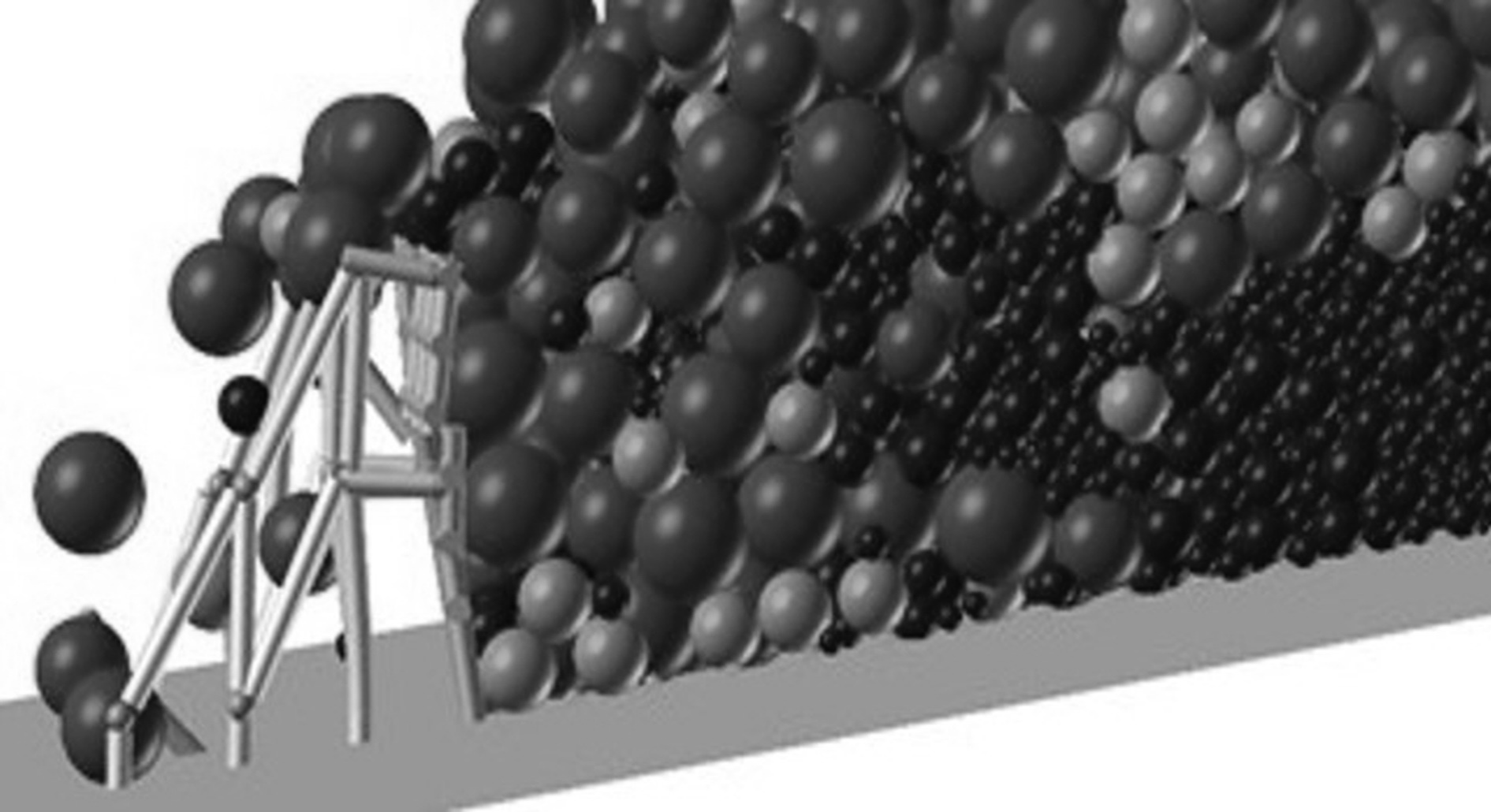

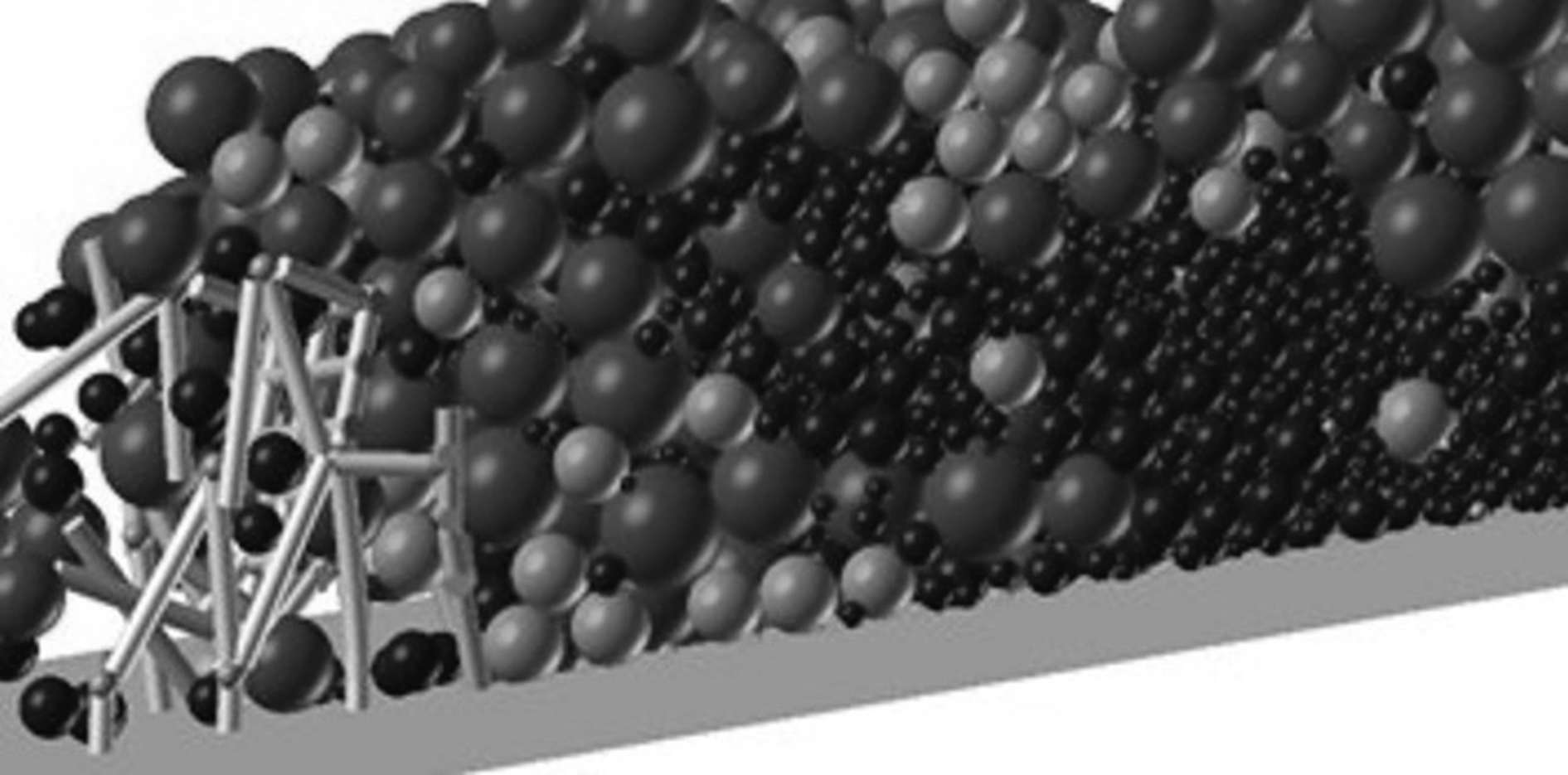

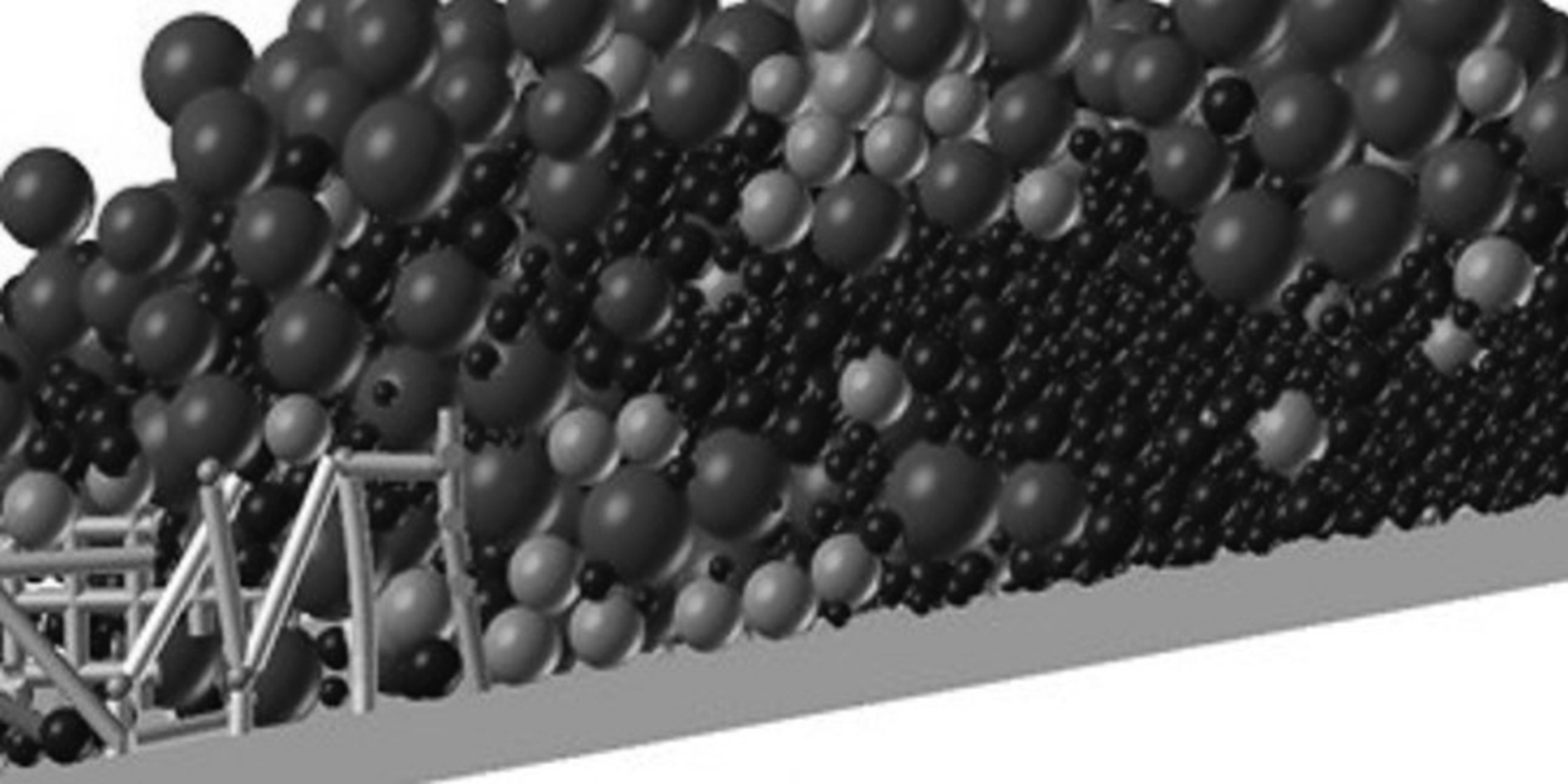

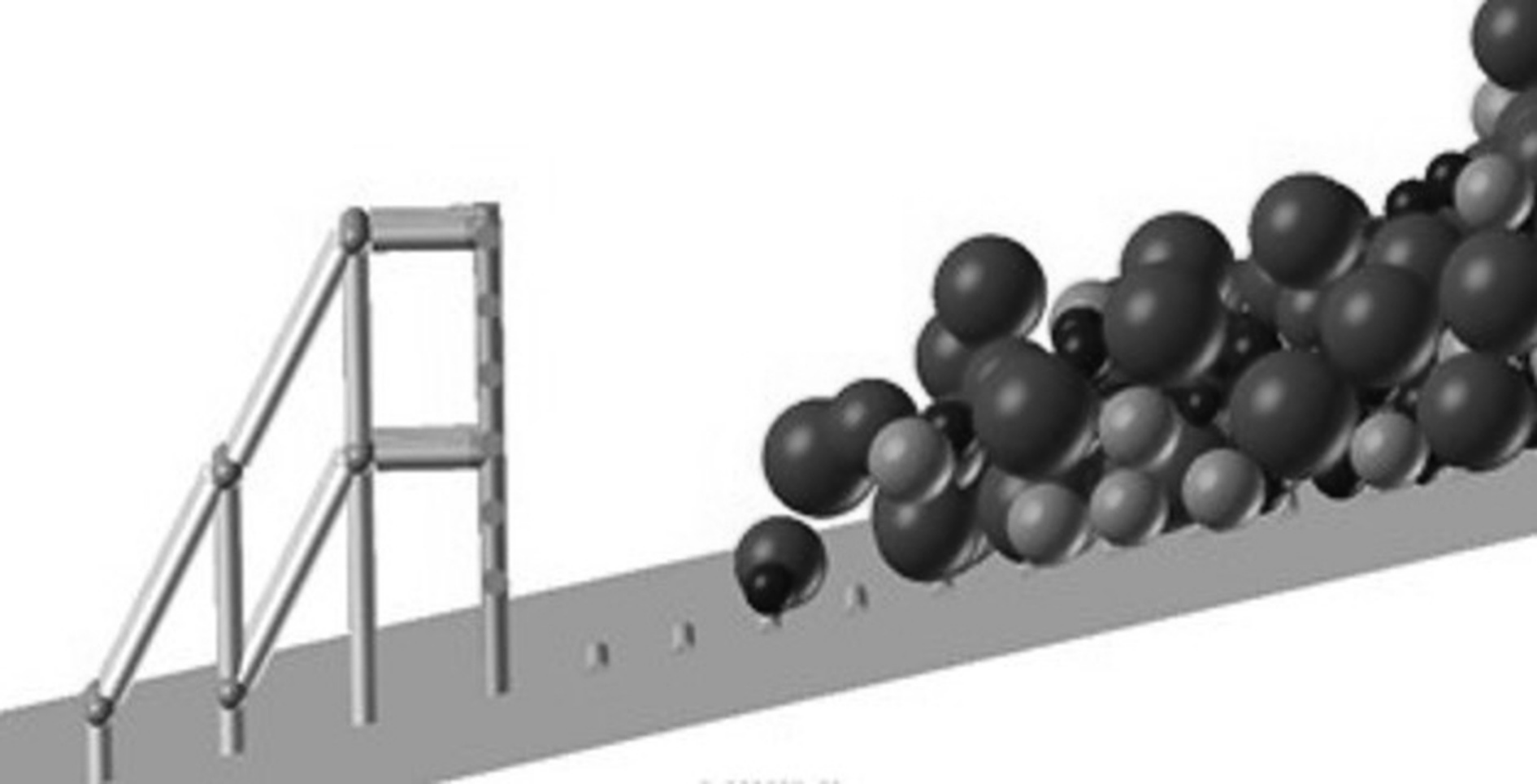

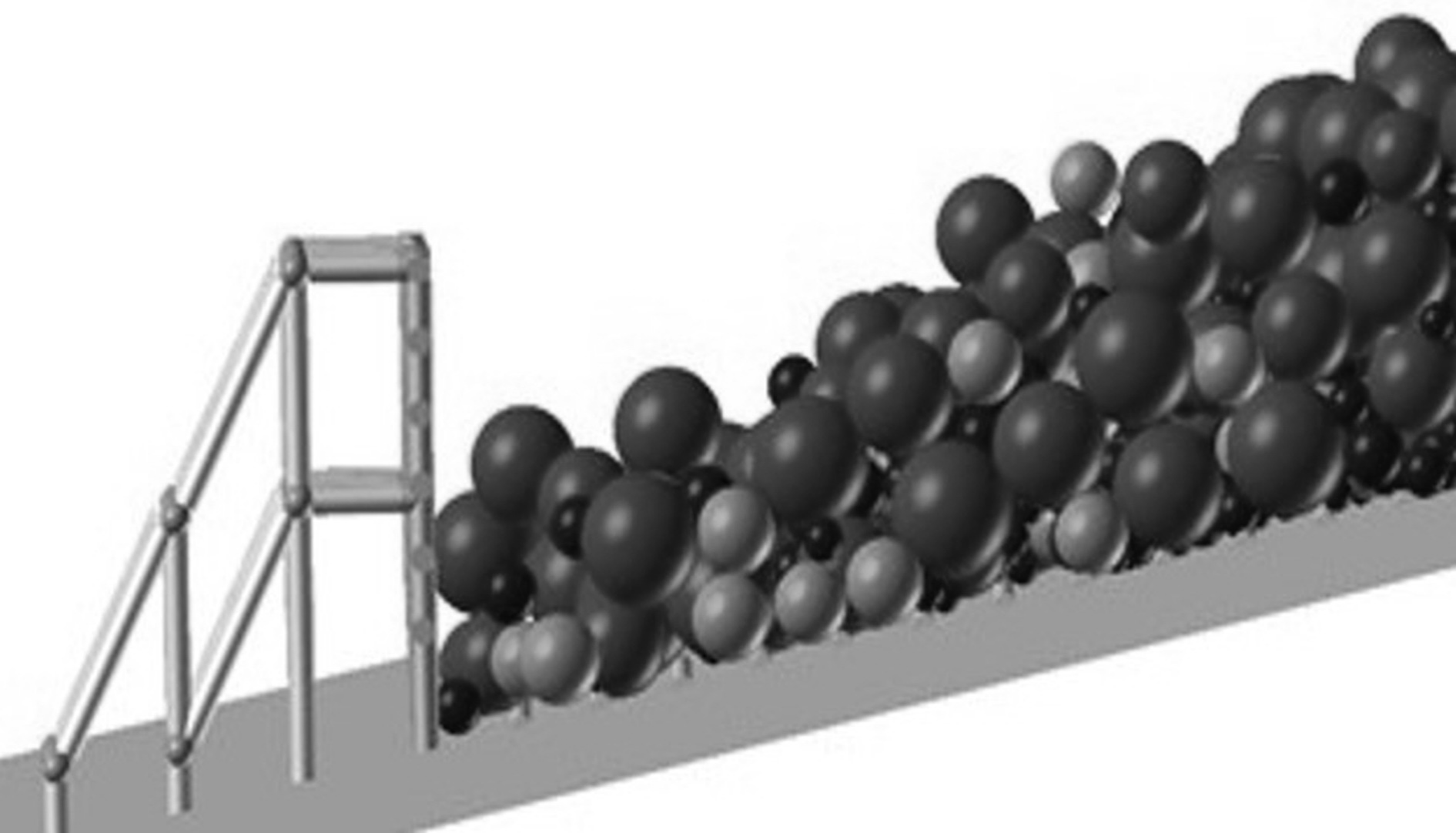

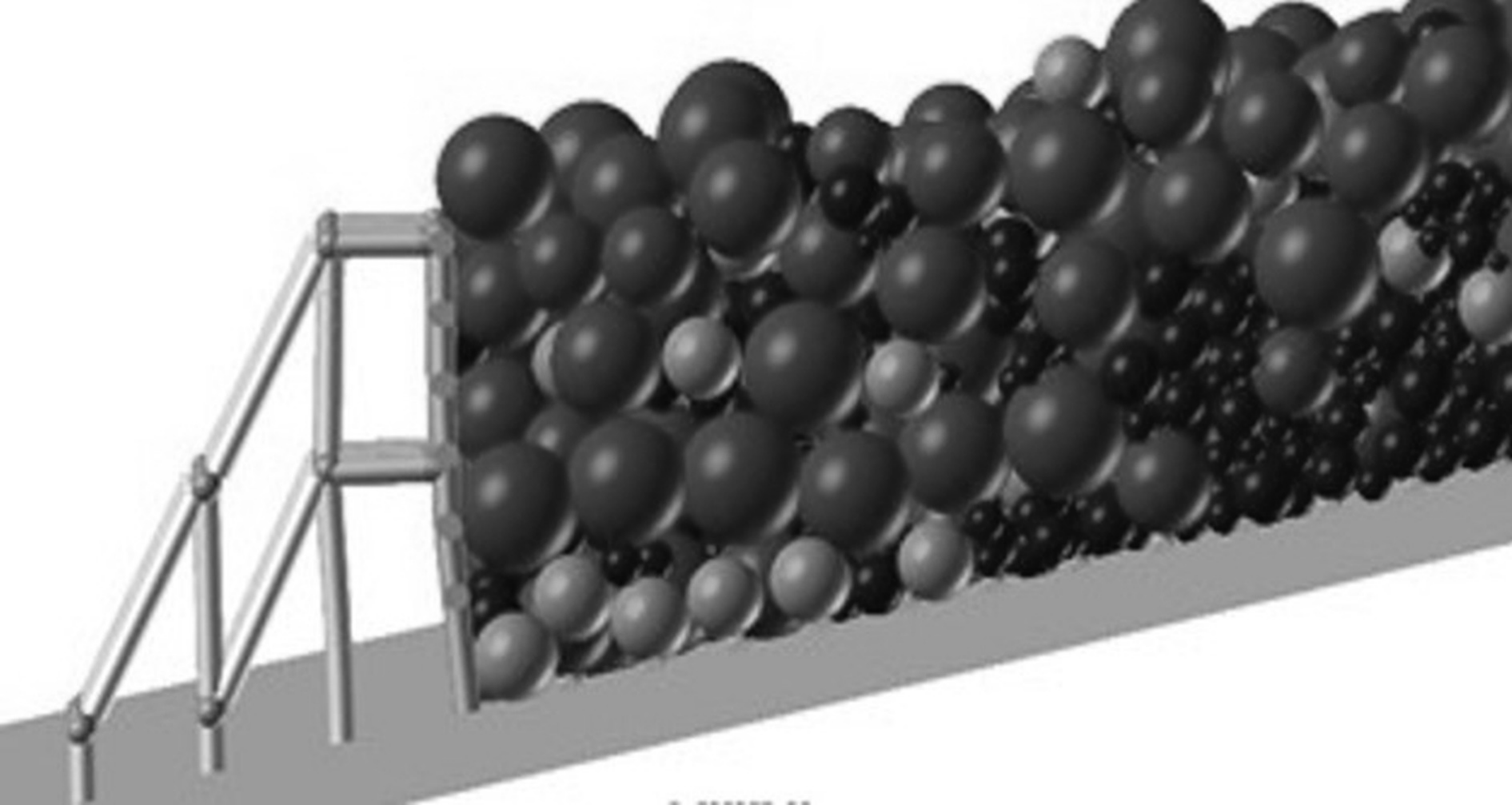

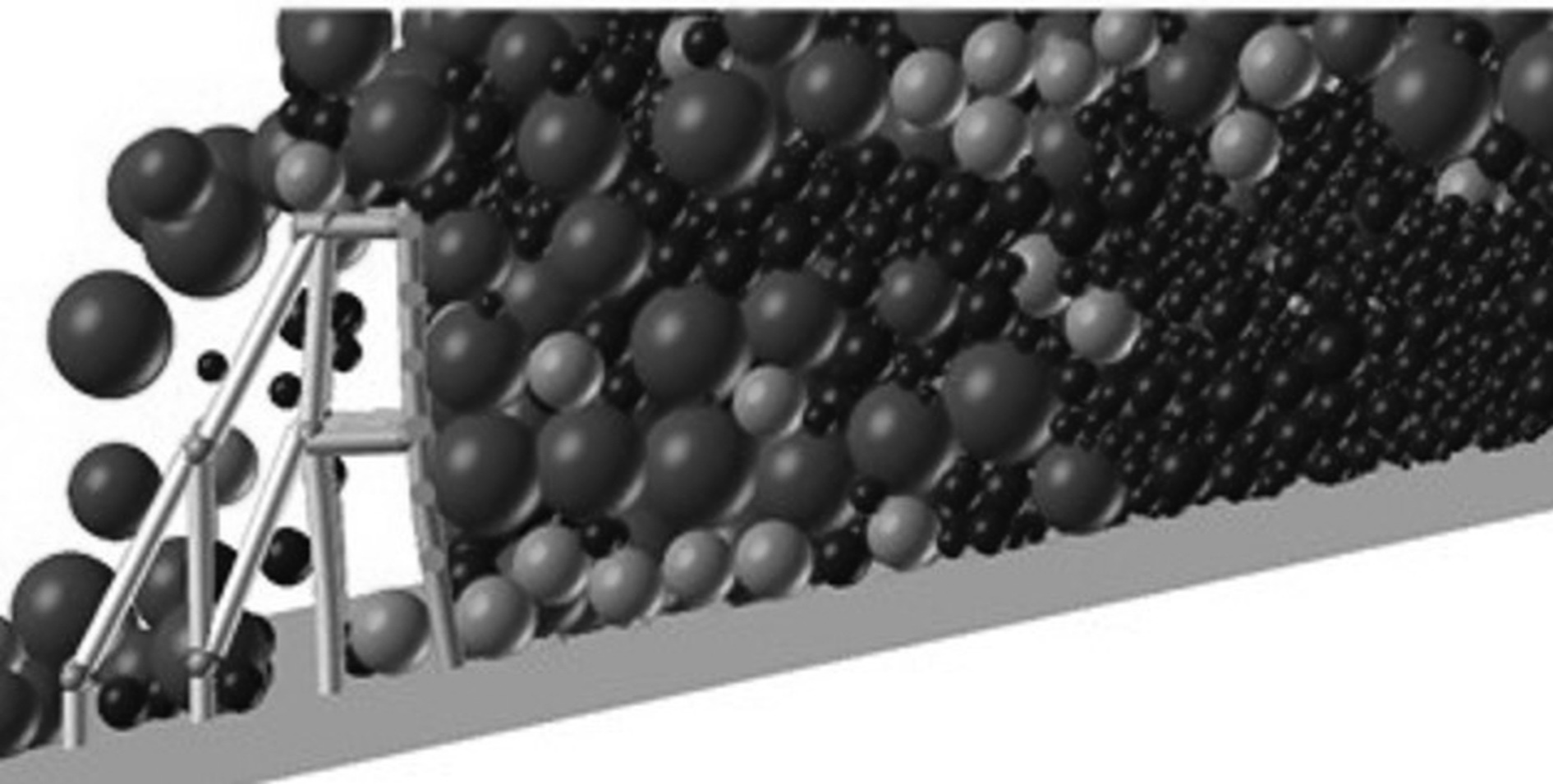

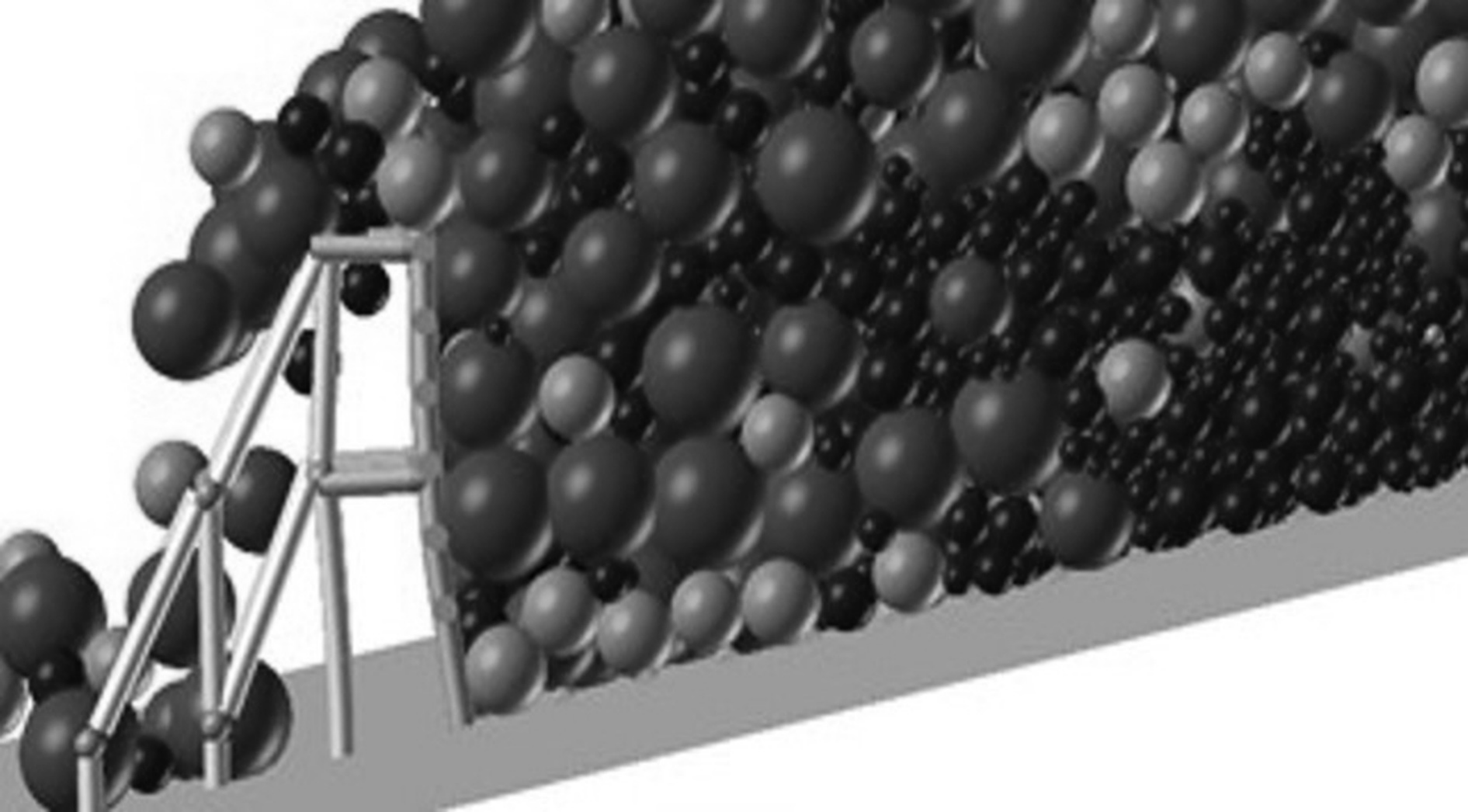

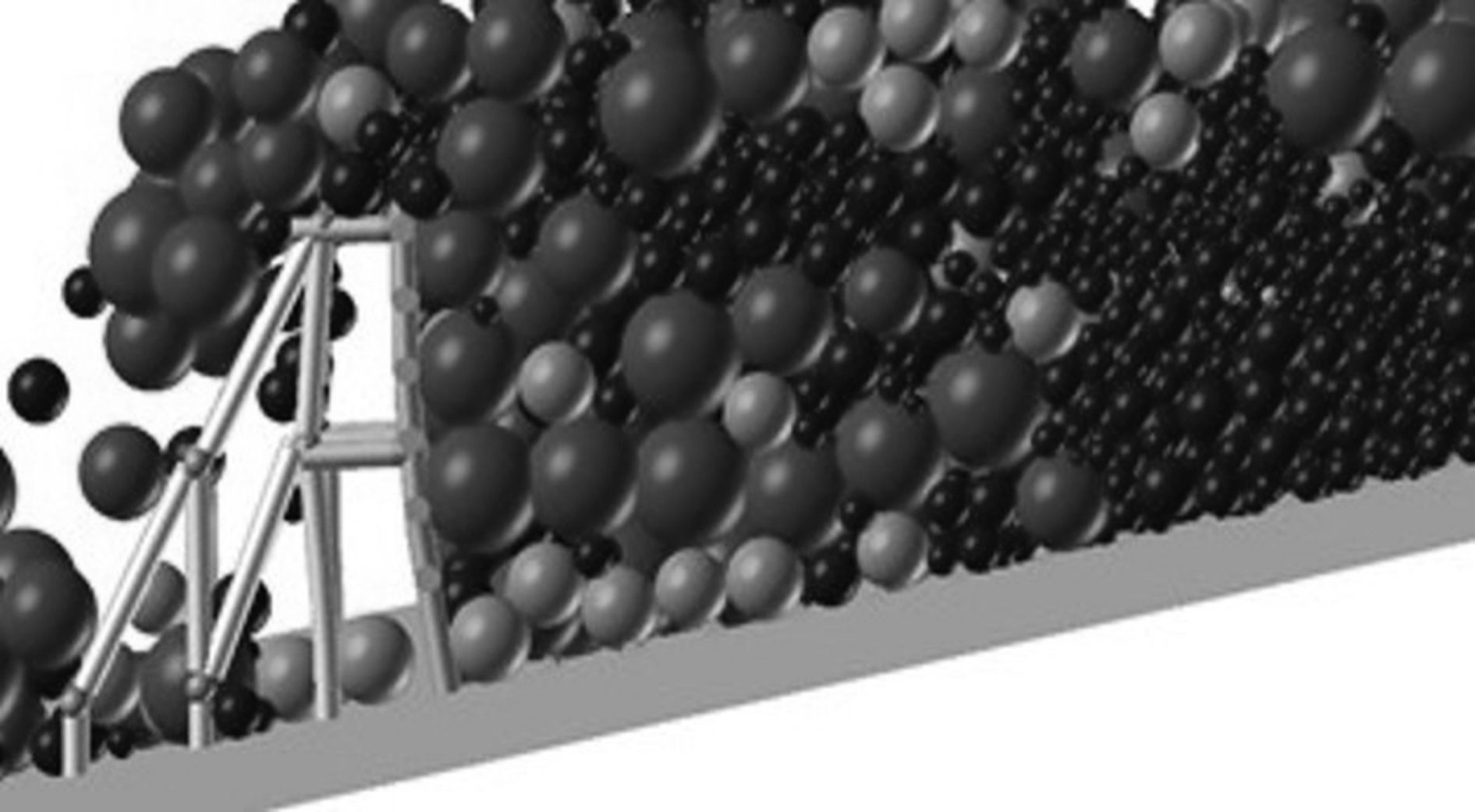

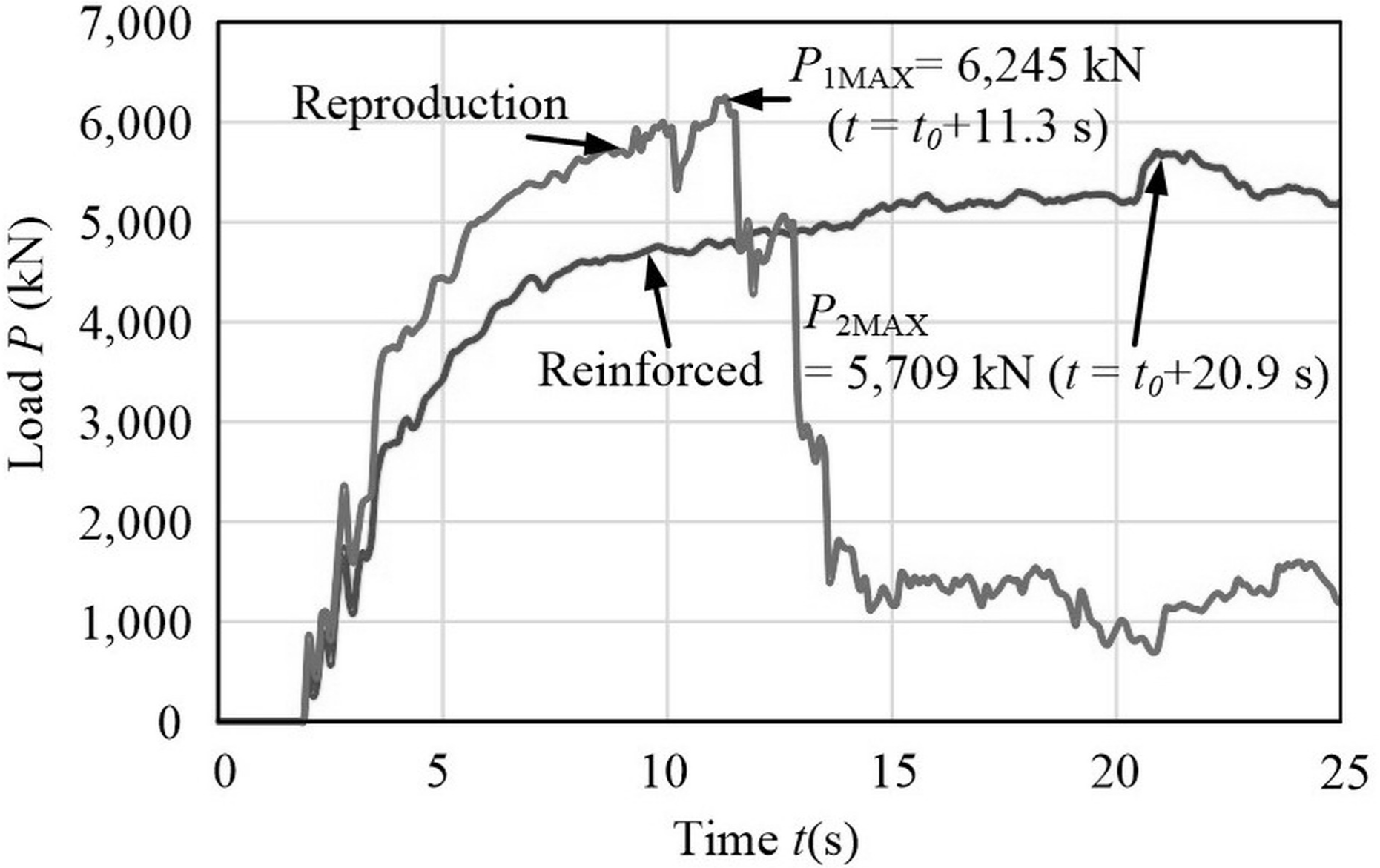
7,000
6,000
5,000
4,000
3,000
2,000
1,000
0
Load P (kN)
0
5
10
15
20
25
Time t(s)
Reproduction
P1MAX= 6,245 kN
(t = t0+11.3 s)
Reinforced
P2MAX
= 5,709 kN (t = t0+20.9 s)

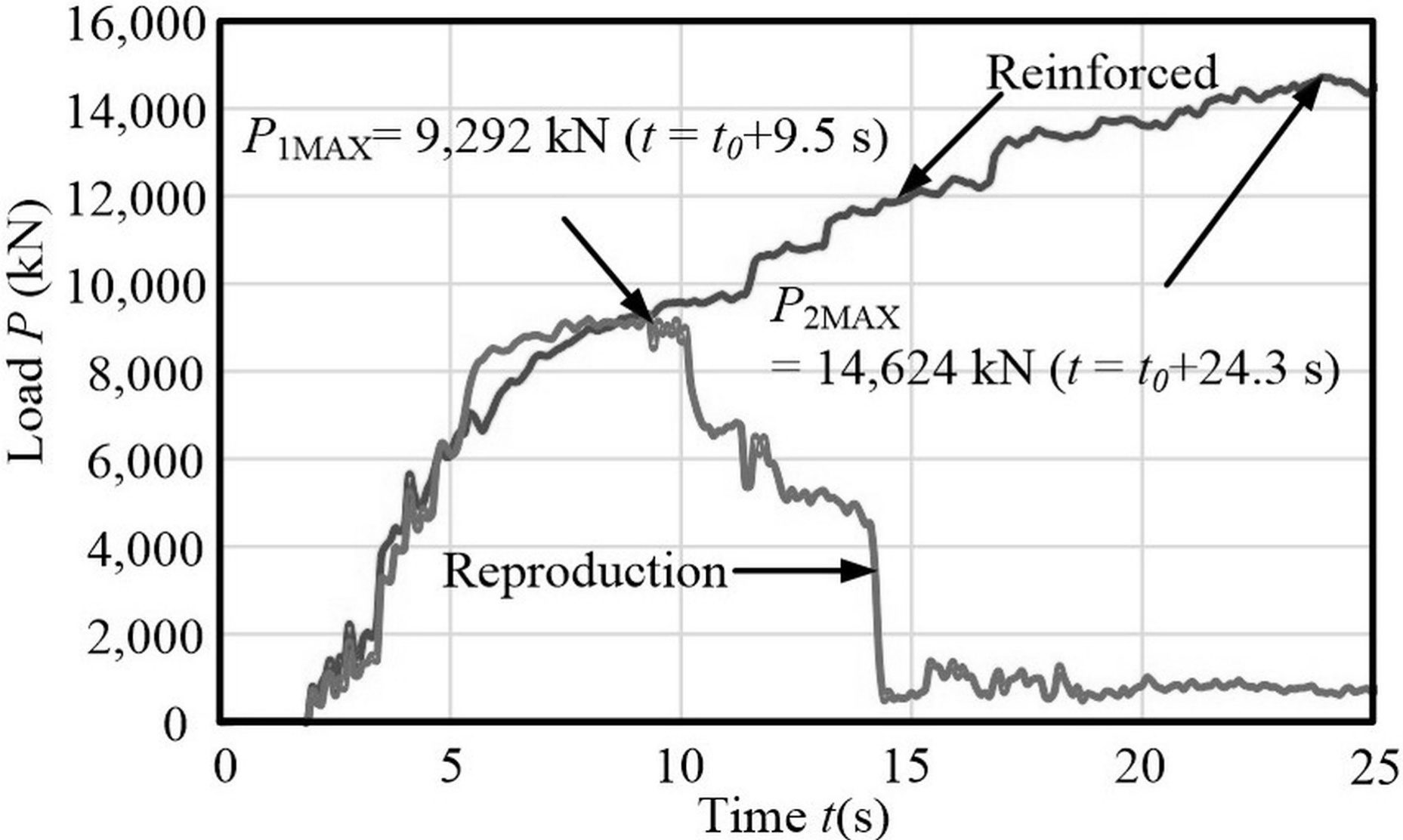
16,000
14,000
12,000
10,000
8,000
6,000
4,000
2,000
0
Load P (kN)
0
5
10
15
20
25
Time t(s)
Reinforced
P1MAX= 9,292 kN (t = t0+9.5 s)
P2MAX
= 14,624 kN (t = t0+24.3 s)
Reproduction

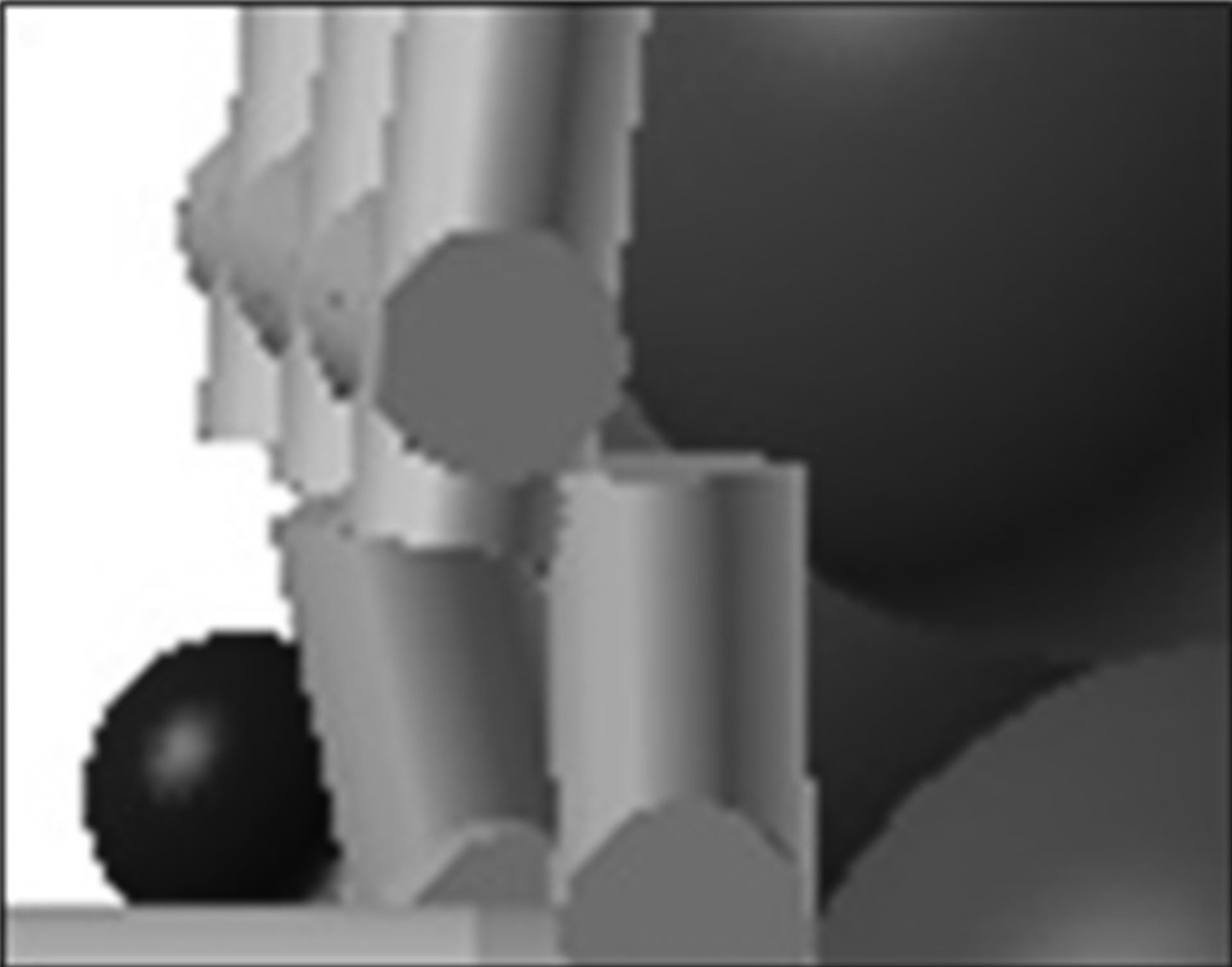

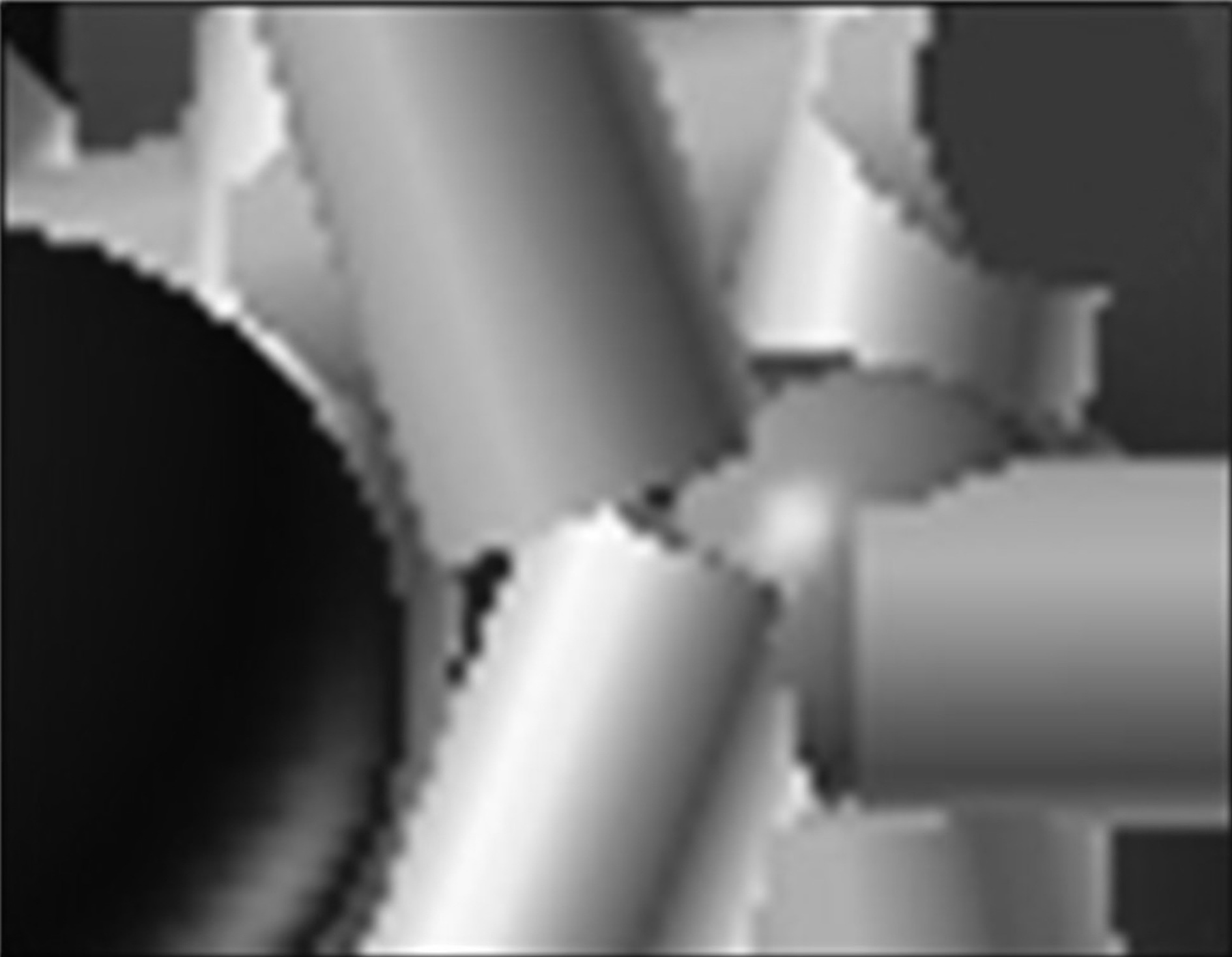

Table 1. Data of debris flow in design and after the debris flow disaster site investigation

	Design (under disaster)	Estimation debris flow (after site investigation)
Gradient of river bed	1/5（11.3 °）	
Unit weight of boulder	25.48 kN/m^3	
Unit weight of water	11.76 kN/m^3	
Unit weight of debris flow	16.42 kN/m^3	
Maximum boulder diameter（D_{95}）	1.1 m	1.6 m
Maximum boulder diameter（D_{max}）	—	6.5 m
Debris flow peak discharge	167.9 m^3/s	730 m^3/s
Debris flow velocity	7.01 m/s	9.7 m/s
Debris flow depth	1.99 m	3.3 m
Debris flow fluid force	163.8 kN/m	520.6 kN/m

Table 2. Boulder investigation results

Investigation point	D_{max} (cm)	D_{95} (cm)	D_{50} (cm)	Number of boulders
①	375	180	60	202
②	265	120	45	162
③	510	160	50	157
④	250	150	50	152
⑤	215	180	75	106
⑥	190	145	65	100
⑦	240	150	75	200
⑧	170	85	40	200
⑨	270	140	65	200

Table 3. Initial analysis parameters for the analytical element model

Item		Value
Flow	Velocity (m/s)	9.7
	Debris flow depth (m)	3.3
	Drag force coefficient	0.49
Boulder model	Size（20–60 cm）Color : Blue	4,263
	Size（60–100 cm）Color : Blue	3,983
	Size（100–160 cm）Color :Green	1,512
	Size（160–300 cm）Color : Red	609
Between element spring	Normal spring constant, K_n（N/m）	1.0×10^{7}
	Tangential spring constant, K_s（N/m）	3.5×10^{6}
	Viscosity (N)	0
	Damping constant	0.8
	Friction coefficient	0.404
Time increment (s)		1.0×10^{-6}

Table 4. Physical parameters of the open sabo dam

Item		Value
Coupling joint	Axial tension stiffness, EA (N)	1.04×10^{10}
	Bending stiffness, EI (Nm^2)	4.38×10^{7}
	Poisson's ratio	0.3
	Breaking elongation percentage (%)	18
Welding part of hollow steel	Axial tension stiffness, EA (N)	4.0×10^{6}
	Bending stiffness, EI (Nm^2)	2.9×10^{6}
	Poisson's ratio	0.3
	Breaking elongation percentage (%)	95
Hollow steel (t = 22.0 mm)	Axial tension stiffness, EA (N)	4.06×10^{9}
	Bending stiffness, EI (Nm^2)	3.50×10^{8}
	Poisson's ratio	0.3
	Breaking elongation percentage (%)	21
Hollow steel (t = 12.7 mm)	Axial tension stiffness, EA (N)	2.38×10^{9}
	Bending stiffness, EI (Nm^2)	2.12×10^{7}
	Poisson's ratio	0.3
	Breaking elongation percentage (%)	21

Note: t is the thickness of hollow steel pipe.